Protist, Vol. 169, 826–852, December 2018
http://www.elsevier.de/protis
Published online date 28 June 2018

Protist

ORIGINAL PAPER

Fine structure and Molecular Phylogenetic Position of Two Marine Gregarines, *Selenidium pygospionis* sp. n. and *S. pherusae* sp. n., with Notes on the Phylogeny of Archigregarinida (Apicomplexa)

Gita G. Paskerova[a,1], Tatiana S. Miroliubova[a], Andrei Diakin[b], Magdaléna Kováčiková[b], Andrea Valigurová[b], Laure Guillou[c], Vladimir V. Aleoshin[d], and Timur G. Simdyanov[e]

[a]Department of Invertebrate Zoology, Faculty of Biology, Saint Petersburg State University, Universitetskaya emb. 7/9, St Petersburg 199 034, Russian Federation
[b]Department of Botany and Zoology, Faculty of Science, Masaryk University, Kotlářská 2, 611 37 Brno, Czech Republic
[c]Sorbonne Université, Université Pierre et Marie Curie – Paris 6, CNRS, UMR 7144, Station Biologique de Roscoff, Place Georges Teissier, CS90074, 29688 Roscoff Cedex, France
[d]Belozersky Institute for Physico-Chemical Biology, Lomonosov Moscow State University, Leninskie Gory, Moscow 119 234, Russian Federation
[e]Department of Invertebrate Zoology, Faculty of Biology, Lomonosov Moscow State University, Leninskie Gory, Moscow 119 234, Russian Federation

Submitted October 30, 2017; Accepted June 19, 2018
Monitoring Editor: Frank Seeber

Archigregarines are a key group for understanding the early evolution of Apicomplexa. Here we report morphological, ultrastructural, and molecular phylogenetic evidence from two archigregarine species: *Selenidium pygospionis* sp. n. and *S. pherusae* sp. n. They exhibited typical features of archigregarines. Additionally, an axial row of vacuoles of a presumably nutrient distribution system was revealed in *S. pygospionis*. Intracellular stages of *S. pygospionis* found in the host intestinal epithelium may point to the initial intracellular localization in the course of parasite development. Available archigregarine SSU (18S) rDNA sequences formed four major lineages fitting the taxonomical affiliations of their hosts, but not the morphological or biological features used for the taxonomical revision by Levine (1971). Consequently, the genus *Selenidioides* Levine, 1971 should be abolished. The branching order of these lineages was unresolved; topology tests rejected neither para- nor monophyly of archigregarines. We provided phylogenies based on LSU (28S) rDNA and near-complete ribosomal operon

[1]Corresponding author; fax +7 812 3289703
e-mail gitapasker@yahoo.com, g.paskerova@spbu.ru (G.G. Paskerova).

https://doi.org/10.1016/j.protis.2018.06.004

(concatenated SSU, 5.8S, LSU rDNAs) sequences including *S. pygospionis* sequences. Although being preliminary, they nevertheless revealed the monophyly of gregarines previously challenged by many molecular phylogenetic studies. Despite their molecular-phylogenetic heterogeneity, archigregarines exhibit an extremely conservative plesiomorphic structure; their ultrastructural key features appear to be symplesiomorphies rather than synapomorphies.

Key words: Unicellular parasites; polychaetes; ultrastructure; 18S rDNA; 28S rDNA; molecular phylogeny.

Introduction

Apicomplexa is a large group of unicellular parasites infecting a wide range of invertebrate and vertebrate hosts. Some apicomplexans, such as the human pathogens *Plasmodium*, *Toxoplasma*, and *Cryptosporidium*, are well studied. At the same time, basal apicomplexans, archigregarines, agamococcidia, blastogregarines, and protococcidia inhabiting exclusively marine invertebrate hosts and being crucial for our understanding of the evolution of parasitism and evolutionary paths of apicomplexans in general, are still poorly investigated.

Archigregarines (Archigregarinida Grassé, 1953, Apicomplexa Levine, 1970) are unicellular parasites inhabiting marine invertebrates, mostly polychaetes. They are thought to have retained a number of plesiomorphic characteristics from the most recent ancestor of all apicomplexans (Cavalier-Smith and Chao 2004; Cox 1994; Desportes and Schrével 2013; Grassé 1953; Leander 2008a; Leander and Keeling 2003). The most often encountered stage of their life cycle is a trophozoite. It is a relatively large cell usually attached to the host cell by the mucron, an attachment apparatus with organelles of the apical complex typical of the invasive stages (zoites). The mucron participates in myzocytosis, feeding by sucking out the cytoplasmic contents of the host cell into food vacuoles (Cavalier-Smith and Chao 2004; Desportes and Schrével 2013; Schrével 1968; Schrével et al. 2016; Simdyanov and Kuvardina 2007; Wakeman and Horiguchi 2018; Wakeman et al. 2014). The pellicle of archigregarines is organized as a three-layered membrane complex. It is supported by microtubules arranged in one or more subpellicular layers (Desportes and Schrével 2013).

The life cycle of archigregarines, a sequence of gamogony (gamete production) and sporogony (zygote fission for producing sporozoites), is often thought to include asexual cell multiplication in the trophozoite stage – merogony (Adl et al. 2012; Desportes and Schrével 2013; Grassé 1953). Levine (1971) and his followers placed great importance on the presence/absence of merogony in the life cycle for the classification of archigregarines, transferring species without merogony to eugregarines (Levine 1971, 1985; Perkins et al. 2000). On the contrary, Schrével with coauthors considered merogony to be non-important for the high-level classification of archigregarines (Desportes and Schrével 2013; Schrével 1970, 1971a,b; Schrével et al. 2016). This point of view was shared by several contemporaneous authors (Kuvardina and Simdyanov 2002; Leander 2006, 2007; Rueckert and Leander 2009; Rueckert and Horák 2017; Simdyanov and Kuvardina 2007). It should be noted that the absence of merogony is difficult to prove. In this context, taxa delineation should be based on the presence of the easiest observable stage (trophozoites) and morphological characteristics. At present, taxonomy and determination of basic taxonomic characters are routinely determined by electron microscopy and molecular phylogenies.

SSU rDNA-based phylogenetic trees obtained recently are in good accordance with the interpretation that archigregarines are a paraphyletic stem group from which other gregarine lineages evolved (Cavalier-Smith 2014; Cavalier-Smith and Chao 2004; Grassé 1953; Rueckert and Leander 2009; Rueckert and Horák 2017; Schrével et al. 2016; Wakeman and Horiguchi 2018; Wakeman and Leander 2012, 2013; Wakeman et al. 2014). To date, there are more than 70 species of archigregarines. Most of them belong to the genus *Selenidium* (Desportes and Schrével 2013; Levine 1971; Rueckert and Horák 2017; Rueckert and Leander 2009; Wakeman and Horiguchi 2018; Wakeman and Leander 2012, 2013; Wakeman et al. 2014; WoRMS 2018).

Despite their significant molecular-phylogenetic heterogeneity, species of *Selenidium* possess a similar and extremely conservative morphology. It is represented by the morphostasis, a set of characters typical of the invasive stages (zoites)

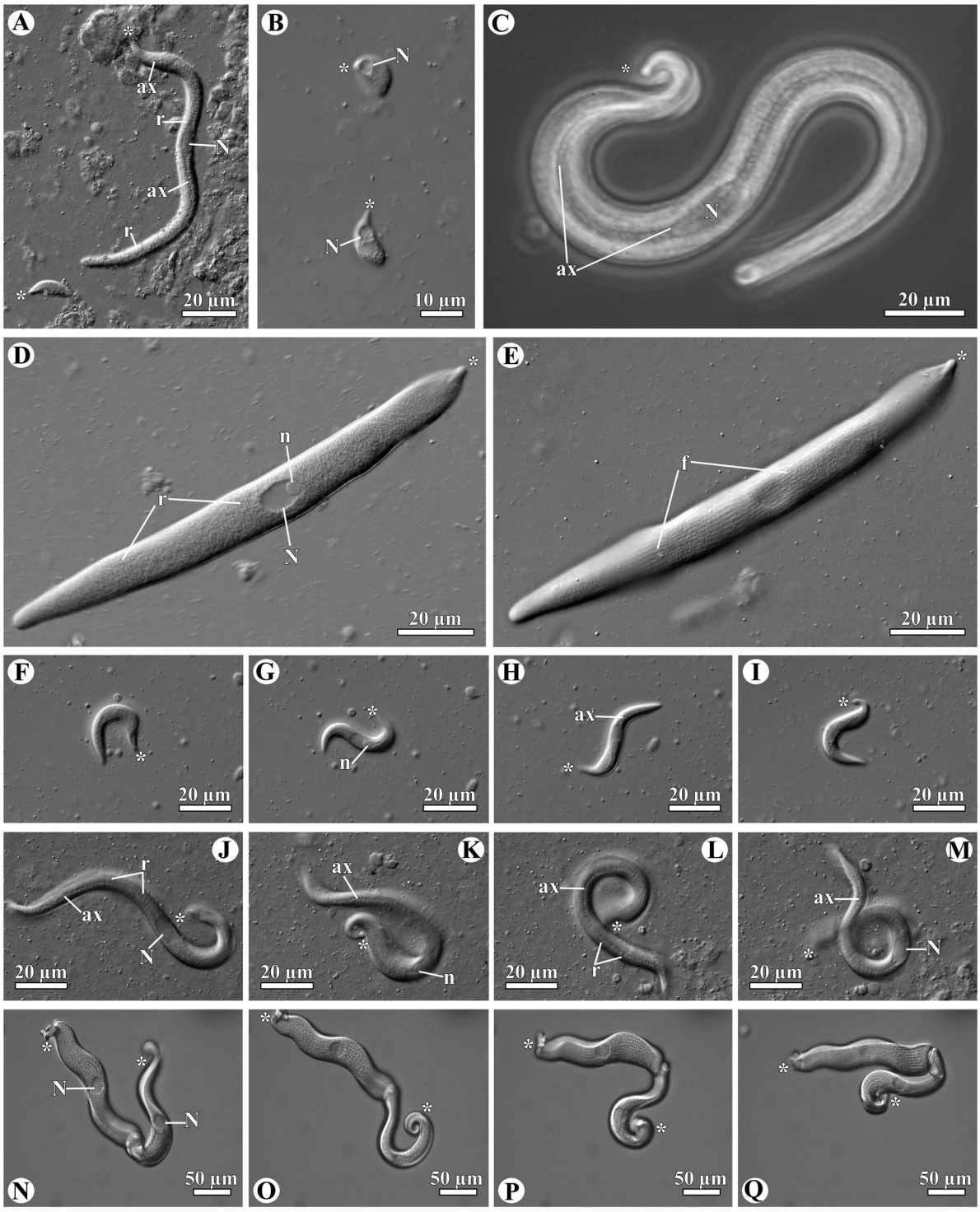

Figure 1. General morphology and motility of S*elenidium pygospionis* sp. n. Differential interference contrast (DIC) and phase-contrast (PH) light micrographs. **A**. Attached large and detached small trophozoites. In the large trophozoite, note the axial streak along the longitudinal cell axis and radial threads running from the axial streak towards the cell periphery. DIC. **B**. Young trophozoite showing bending motility; the composition of two micrographs of the same cell. DIC. **C**. Large trophozoite lying on one of the narrow sides and slightly pressed with the coverslip. Note the axial streak. PH. **D–E**. Large trophozoite lying on one of the flattened sides and pressed with the coverslip; D and E—different optical sections of the same cell. The axial streak is not visible. DIC. **F–I**. Medium-sized trophozoite lying on one of the narrow sides;

of parasitic apicomplexans (Leander and Keeling, 2003). Additionally, molecular phylogenetic studies have repeatedly demonstrated a host-parasite coevolution when closely related archigregarines parasitize closely related hosts (Desportes and Schrével 2013; Rueckert and Horák 2017; Schrével et al. 2016; Wakeman and Leander 2013). Whether these two observations are linked is unknown.

In this study, we report the discovery of two new archigregarine species, *Selenidium pygospionis* sp. n. isolated from spionid polychaetes *Pygospio elegans* and *Polydora glycymerica*, and *S. pherusae* sp. n. isolated from flabelligerid polychaetes *Pherusa plumosa.* We examined the new species using light and electron microscopy, conducted phylogenetic analyses based on the SSU rDNA and obtained the first LSU rDNA sequences of archigregarines.

Results

Selenidium pygospionis sp. n.

Occurrence

The gregarine *Selenidium pygospionis* sp. n. was found in the intestine of the polychaete *Pygospio elegans* (Spionidae) collected at the silty-sand intertidal zone of the White Sea. There were 109 infected polychaetes out of the 302 dissected. The intensity of infection usually varied from 1 to 50 (mode = 1, average = 9.8) gregarines per host; in two cases, the number of parasites reached 100 and 150 cells per host. Both attached and non-attached trophozoites of different sizes were found in the host intestine (Fig. 1A). Syzygies were extremely rare (a few in all dissected polychaetes). In squash preparations (see Methods) of more than 100 examined polychaetes, no other stages of the life cycle (gametocysts or stages of merogony) were observed.

We also found very similar parasites in the intestine of the shell-boring polychaete *Polydora glycymerica* (Spionidae) inhabiting the bivalve *Glycymeris yessoensis* from the Sea of Japan. The intensity of infection was about 30 parasites per host.

Parasites isolated from polychaetes of both species were identical in their morphology, fine structure, and DNA sequences. Therefore, we considered them to belong to the same species. Further description of *S. pygospionis* was predominantly based on the evidence obtained from the White Sea samples as the most representative ones.

General Morphology

As shown with light microscopy (LM) and scanning electron microscopy (SEM), trophozoites *S. pygospionis* were anchored in the host tissue with their anterior end (Figs 1 A, 2 A, B). The parasites were easy to dislodge from the intestinal epithelium during the dissection of the hosts.

The smallest trophozoites, presumably young trophozoites not long after their transformation from zoites (most likely, sporozoites), were observed occasionally. They were spindle-shaped with a pointed anterior end and a rounded posterior end. Their length varied from 15 to 23 μm (n = 2), and their width, from 6 to 7 μm (n = 2) in the middle part of the cell. A single rounded nucleus was located in the anterior half of the cell. The parasites could bend slightly in one plane but never glided (Fig. 1B).

Well-developed trophozoites were elongated, vermiform and slightly flattened (Figs 1 C–M, 2 C, D). Their length varied from 34 to 288 μm (average 144 μm, mode 146 μm, n = 79); their maximum width (4–25 μm, average 12 μm, mode 11 μm, n = 76) was in the middle of the cell where an oval nucleus [6–22 μm (av. 17 μm, n = 40) × 5–11 μm (av. 8.4 μm, n = 26)] was located. The nucleus was elongated along the longitudinal axis of the cell (Fig. 1A, C, D). A single spherical nucleolus (3.1–6.3 μm, n = 6) was commonly situated at the anterior pole of the nucleus (Fig. 1D). The anterior end of the parasites was usually hook-like, bent in the median plane (the plane perpendicular to the flattened sides) towards one of the flattened sides of the cell (Figs 1 C–E, 2 C, D). The mucron was dome-shaped with a smooth surface. In some individuals, it had a small pit in the center (Fig. 2C). The posterior end was rounded (Fig. 2D). The entire surface bore 22–30 (n = 12), usually 28, broad and low folds separated by grooves (Figs 1 E, 2 B–E).

a series of micrographs illustrating bending motility (1–2 bends along the cell). DIC. **J–M**. Large trophozoite lying on one of the narrow sides; a series of micrographs illustrating bending motility (2–3 bends along the cell). Note the coiling of the anterior end (K). DIC. **N–Q**. Syzygy; a series of micrographs illustrating bending motility (up to 4 bends along the cell) and the coiling of the anterior end. The axial streak is not visible. DIC. *, anterior end; ax, axial streak; f, folds; N, nucleus; n, nucleolus; r, radial threads.

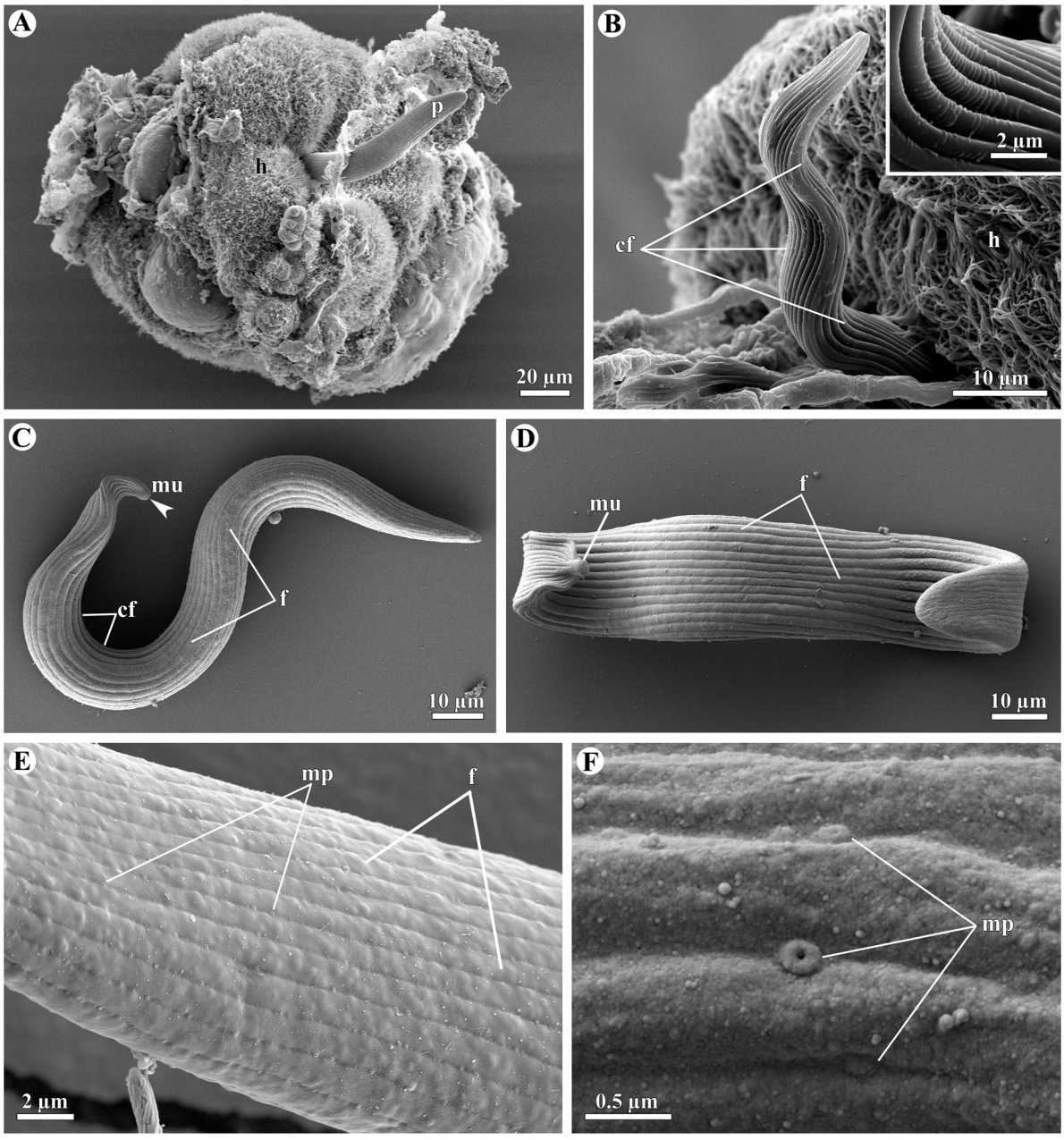

Figure 2. Surface morphology of S*elenidium pygospionis* sp. n. Scanning electron micrographs. **A**. Trophozoite attached to a fragment of the host intestinal epithelium by its anterior end. **B**. Attached trophozoite with three bends of its cell. Note small transversal compression folds of the parasite's pellicle at the inner surface of each bend. **Inset**. Transversal compression folds at high magnification. **C–D**. Detached trophozoites lying on one of the narrow sides (C) and one of the wide sides (D) of their cells. Note a hook-bent anterior end with a smooth, dome-shaped mucron, and folds at the cell surface. The arrowhead points to the pit at the center of the mucron in C. **E**. Micrograph of the trophozoite surface showing the number and location of micropores (mp). **F**. Micropore at high magnification. cf, transversal compression folds; f, folds; h, host intestinal epithelial tissue; mu, mucron; mp, micropores; p, parasite.

The width of the folds varied from 0.5 to 1.5 μm (av. 0.9, n = 21) in archigregarines fixed according to different protocols (Fig. 2D, E). Numerous micropores (10–20 per 50 μm^2, n = 2) were observed at the bottom of the grooves; their edges were slightly raised above the cell surface (Fig. 2E, F). The outer and the inner diameter of the micropores was 134–287 and 38.5–74.6 nm (n = 6), respectively.

LM studies showed that well-developed trophozoites had an intracellular axial streak of optically distinct cytoplasm extending from the anterior end to the posterior end and forming an expansion around the nucleus. Numerous radial threads ran from the axial streak towards the cell periphery. The axial streak was easy to observe in trophozoites lying on one of the narrow sides (Fig. 1A, C, H, J–M).

Both attached and non-attached cells performed very active bending movements in the median plane (Fig. 1A, C, F–M, and Supplementary Material Video S1). Non-attached archigregarines usually moved non-progressively on one of their narrow sides along the substrate. Medium-sized trophozoites usually formed 1–2 bending sections along the cell, while large-sized ones combined 2–4 bends with coiling of their anterior end (Fig. 1F–I vs J–Q). Bending and coiling of the cell always started at the hook-like anterior end. Fixed archigregarines usually retained the bends of their body resulting from their motility (Fig. 2A–D). There were small transversal compression folds of the pellicle at the inner surface of each bend (Fig. 2B, C). In addition, the trophozoites of *S. pygospionis* never shortened along their anterior-posterior axis.

Syzygies were caudal when two gamonts coupled with their posterior ends. The syzygy partners moved asynchronously (Fig. 1N–Q, Supplementary Material Video S2).

Fine Structure

Transmission electron microscopic (TEM) studies showed that the trophozoite tegument was represented by a trimembrane pellicle [the plasma membrane and the inner membrane complex (IMC)] (Fig. 3 A). The IMC consisted of the external and the internal cortical cytomembrane separated from each other by an electron-transparent space (8–10 nm thick), while the plasma membrane was separated from the IMC by a space of higher electron density (12–14 nm thick). The thickness of the pellicle varied from 36 to 40 nm. The cell coat (glycocalyx) covering the parasite surface was poorly visible. The pellicle was underlain by longitudinally oriented subpellicular microtubules (Fig. 3A–D). They were arranged in a single layer, the continuity of which was interrupted under the grooves where micropores were usually located. Additionally, groups of irregularly arranged microtubules were present under the main layer. Each microtubule was surrounded by an electron-transparent sheath of the cell cytoplasm (Fig. 3A). Micropores were present as invaginations of the plasma membrane. Each invagination was surrounded with a thick cylindrical structure, formed by the cytomembranes of the IMC, and some electron-dense substance (Fig. 3A, inset). Numerous vesicles with some multi-membranous whorls or dense material inside were incorporated in the microtubule layer and the inner membrane complex of the pellicle; they were connected with the plasma membrane (Fig. 3C, D).

It could be seen in ultrathin sections of trophozoite-infected intestines that the anterior end of *S. pygospionis* was inserted between folds of the host intestinal epithelium (Fig. 3E, F). There was no direct contact between the host cell and the attached parasite in any of the examined cases. Several rhoptries and numerous groups of putative micronemes were present in the cytoplasm of the anterior end (Fig. 3E). The basal part of the conoid, several ducts of rhoptries within the conoid, and a large mucronal vacuole containing some loose fibrillar material could be seen in some tangential sections through the mucron (Fig. 3F).

The cytoplasm of the trophozoites was indistinctly differentiated into two areas: the ectoplasm and the endoplasm. The former was a narrow cortical region containing subpellicular microtubules, numerous mitochondria arranged at the peripheral layer and vesicles with some multi-membranous whorls or dense material under grooves. The endoplasm, the rest of the cytoplasm, contained a large nucleus, numerous amylopectin granules, lipid droplets, some small electron-dense bodies, and a few mitochondria (Fig. 3G, H). The distribution of organelles and inclusions in the endoplasm was irregular. Narrow, electron-light spaces without any visible organelles could be seen around the nucleus, along the cell axis and perpendicular to it (Figs 3 G–I, 4 B, C). In addition, a series of differently-sized vacuoles was arranged along the cell axis in front and behind the nucleus in the endoplasm. Some of them were linked to each other by membrane tunnels. The content of these vacuoles was mainly electron-transparent with a small amount of some loose filamentous material (Fig. 4 A–C). Small vacuoles of similar appearance also surrounded the nucleus alongside with an electron-transparent area of the cytoplasm (Fig. 4B, inset).

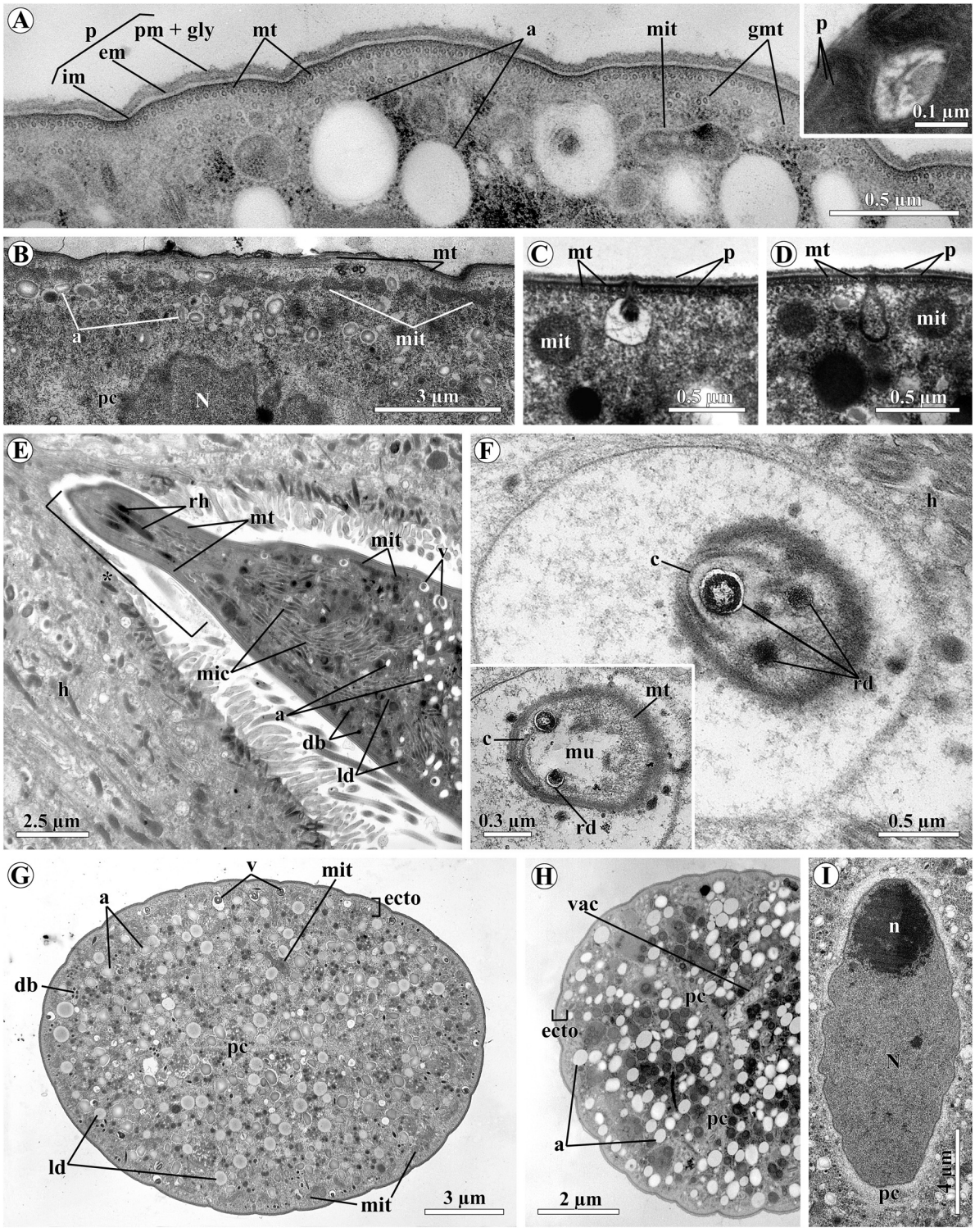

Figure 3. Fine structure of *Selenidium pygospionis* sp. n. Transmission electron micrographs. **A**. Transverse section showing details of the cortex organization. **Inset**. Micropore at high magnification. **B**. Superficial longitudinal section of a trophozoite showing the layer of longitudinal microtubules and the layer of mitochondria under the pellicle. **C–D**. Transversal sections of the pellicle showing vesicles inserted in the microtubule layer and the inner membrane complex. **E**. Superficial longitudinal section of the anterior end of a trophozoite inserted

As shown in a SEM study of de-paraffinized histological sections of *P. elegans*, some gregarines were deeply embedded in the intestinal epithelium almost reaching the basal lamina (Fig. 4D–E).

TEM observations of ultrathin sections revealed that some small single trophozoites (up to 40 μm in length) were localized intracellularly within parasitophorous vacuoles (Fig. 4F–G). The organization of these individuals was generally identical to that of well-developed trophozoites (Fig. 4F, G). The internal space of the parasitophorous vacuole was electron-transparent and filled with filamentous material and electron-dense granules. The density of their arrangement increased towards the periphery. In some sections, there were agglomerations of the electron-dense granules near the parasitophorous vacuole membrane (Fig. 4G, inset). Parasitophorous vacuoles were surrounded on the outside by electron-dense fibrillar material, membranes of endoplasmic reticulum, numerous mitochondria, and cytoplasmic vesicles with multilaminar inclusions, whereas the rest of the host cytoplasm was electron-transparent with rare organelles and vesicles (Fig. 4F–G).

Selenidium pherusae sp. n.

Occurrence

Five polychaetes *Pherusa plumosa* collected at the sublittoral zone of the Sea of Japan were dissected. All of them were infected with *S. pherusae* sp. n. Trophozoites were all localized in the host midgut. Up to several tens of trophozoites per host were found in four of the worms, while the fifth harbored more than 100 trophozoites. No other stages were observed.

General Morphology

S. pherusae trophozoites were attached to the host intestinal epithelium by their anterior end, but were easy to dislodge during the dissection of the hosts.

The trophozoites were elongated, vermiform, 38–269 μm (n = 6) in length and 10–18 μm (n = 4) in maximum width. The anterior end was narrowed and slightly truncated (Fig. 5A, B), while the posterior one was usually rounded in large individuals (Fig. 5A, B) or pointed in small trophozoites (Fig. 5C, D). A spherical nucleus (11–12 μm, in two large trophozoites of 215 and 269 μm in length) was located in the posterior half of the trophozoite, in the widest part of the cell. It contained one nucleolus, 3–5 μm (Fig. 5A, B). Trophozoites had neither longitudinal pellicular folds at the surface nor the axial streak in the cytoplasm (Fig. 5A–C).

Both attached and non-attached gregarines showed a bending motility of the entire cell, usually one bend along the cell at a time. During bending, transient transverse folds formed on the inner surface of the bent part of the cell (Fig. 5A, B). Some fixed gregarines were slightly helically twisted along the longitudinal cell axis (Fig. 5D).

Fine Structure

The tegument of *S. pherusae* had almost the same structure as that of *S. pygospionis*, but the pellicle seemed smooth, without any grooves or folds (Figs 5, 6). Its thickness varied from 33 to 44 nm. The plasma membrane and both cortical cytomembranes were separated from each other by electron-transparent spaces of a similar thickness (7–11 nm). The cell coat was poorly visible (Fig. 6A, C–E). Though the trophozoite surface seemed to be smooth (Fig. 5C, D), micropores were sometimes observed in transverse sections (Fig. 6D, E). They were also similar in structure and size, about 80 μm wide at the surface and 150 μm deep (Fig. 6E). Although the subpellicular microtubules were usually poorly preserved in the ultrathin sections because of fixation artefacts, it could be seen in some sections that they were organized in an uninterrupted layer under the pellicle (Fig. 6C).

between the folds of the host intestinal epithelium. **F**. Oblique-transverse section of the mucron of a trophozoite inserted between the folds of the host intestinal epithelium. **Inset**. Another section of the cell shown in F. **G–H**. Transverse sections of the pre-nuclear (G) and post-nuclear (H) parts of trophozoites showing an indistinct division of the cytoplasm into the ectoplasm at the periphery and the endoplasm occupying the remaining cell volume. Note an electron-light space of the cytoplasm (pc) not containing any visible organelles. Total number of folds in G is 25. **I**. Longitudinal section showing the nucleus. Note an electron-light area of the cytoplasm around the nucleus. *, anterior end; a, amylopectin granules; c, conoid; db, dense bodies; ecto, ectocyte; em, external cytomembrane; gmt, group of microtubules; gly, glycocalyx; h, host tissue; im, inner cytomembrane; ld, lipid droplets; mic, micronemes; mit, mitochondria; mt, microtubules; mu, mucronal vacuole; N, nucleus; n, nucleolus; p, pellicle; pc, electron-light area of the cytoplasm; pm, plasma membrane; rd, ducts of rhoptries; rh, rhoptries; vac, vacuole; v, vesicles with multi-membrane whorls or dense material.

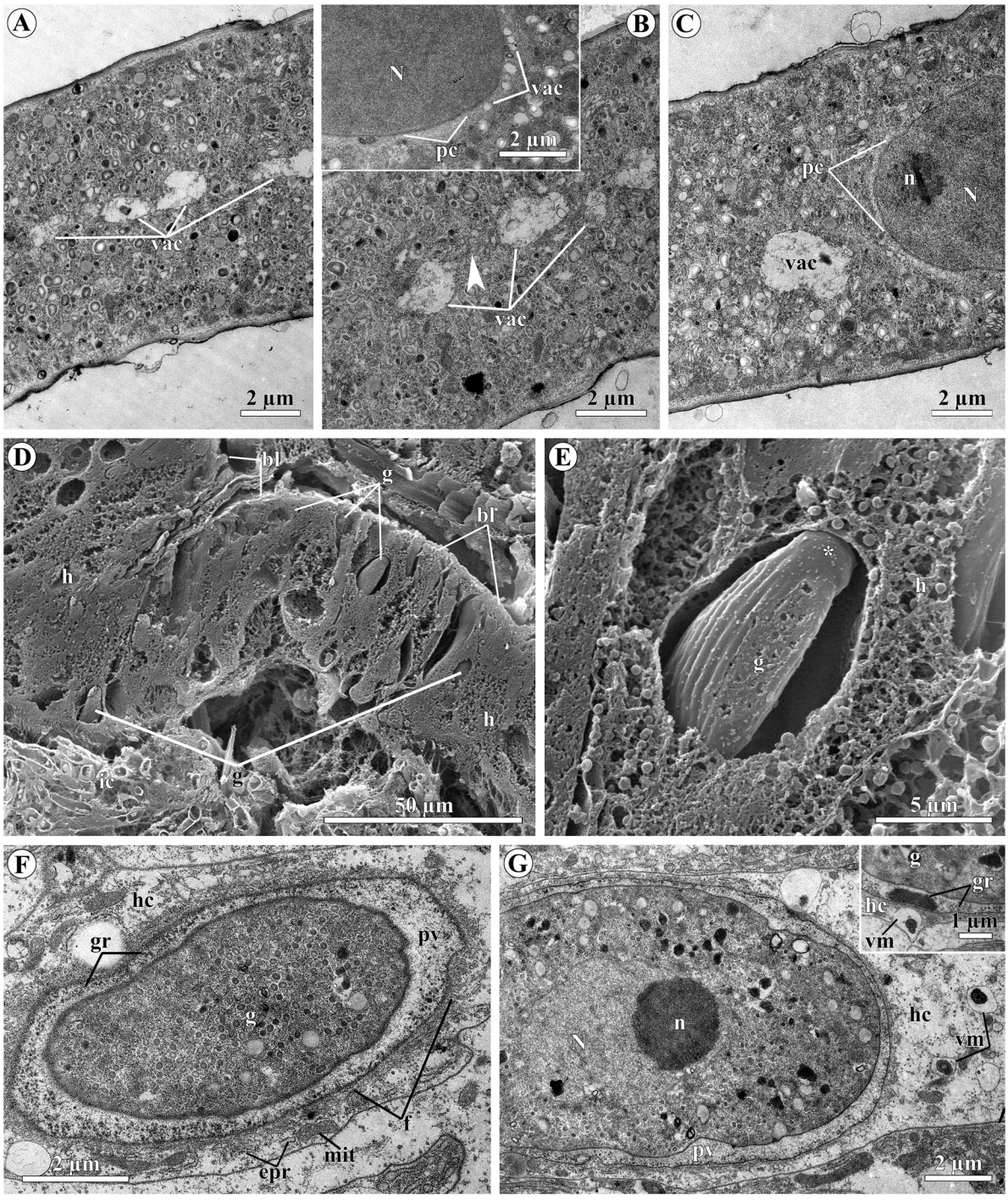

Figure 4. *Selenidium pygospionis* sp. n.: organization of the cytoplasm, localization in the host epithelium, intracellular stage. Transmission (TEM) and scanning (SEM) electron micrographs**. A–C**. Longitudinal thin sections of the trophozoites in the regions where the nucleus is localized showing a series of connected vacuoles along the cell axis. TEM. **Inset in B**. Electron-light area of the cytoplasm around the nucleus with small vacuoles. TEM. **D**. Sagittal histological section of an infected host showing well-developed trophozoites and the degree of their embedding in the host intestinal epithelium. SEM. **E.** Fragment of D at higher magnification. SEM. **F–G**. Superficial oblique thin section (F) and nearly longitudinal thin section (G, inset) showing intracellular stages of the trophozoite development. TEM. **Inset in G**. Agglomeration of electron-dense granules in the parasitophorous vacuole and a vesicle with myelin-like structures in the

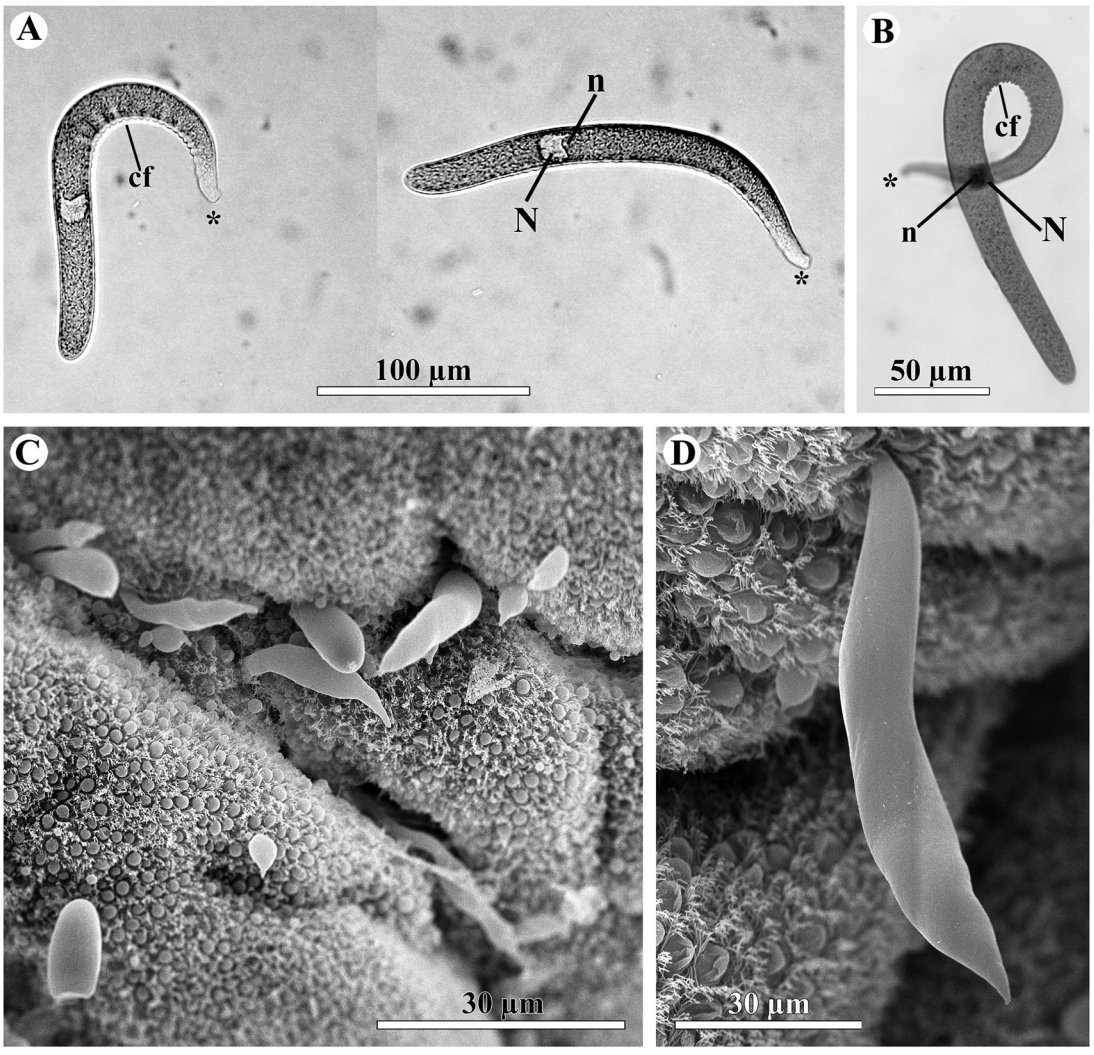

Figure 5. General morphology and motility of S*elenidium pherusae* sp. n. Light microscopic (LM) and scanning electron (SEM) micrographs. **A**. Detached trophozoite showing bending motility; a composition of two micrographs of the same cell. LM. **B**. Detached trophozoite fixed and stained with Carazzi's hematoxylin. LM. **C–D**. Differently sized trophozoites attached to the host intestinal epithelium. SEM. *, anterior end; cf, transversal compression folds; N, nucleus; n, nucleolus.

A truncated and asymmetrical mucron of the parasites formed an extended (up to 4 µm long) zone of cell junction with the host cell (Fig. 6A, C). This junction was represented by a gap 10–30 nm wide. The polar ring, the conoid, several rhoptries and micronemes were observed (Fig. 6A, B). The conoid was a truncated hollow cone consisting of 6–7 spirally arranged microtubules. It measured about 200 nm in height, 286 nm in apical diameter, and 514 nm in basal diameter. The IMC terminated near the apical end of the conoid, where there was a polar ring, adjacently located to the IMC. Sub-

host cell cytoplasm near the membrane of the parasitophorous vacuole. TEM. *, anterior end; arrowhead, membrane tunnel between two vacuoles; bl, basal lamina of the host intestinal epithelium; epr, membranes of the rough endoplasmic reticulum in the host cell; g, archigregarine; gr, electron-dense granules; h, host intestinal epithelium; hc, host cell; ic, intestinal contents; N, nucleus; n, nucleolus; mit, host cell mitochondria; f, fibrils in the host cell; pc, electron-light area of the cytoplasm; pv, parasitophorous vacuole; vac, vacuoles; vm, vesicles with multilaminar inclusions.

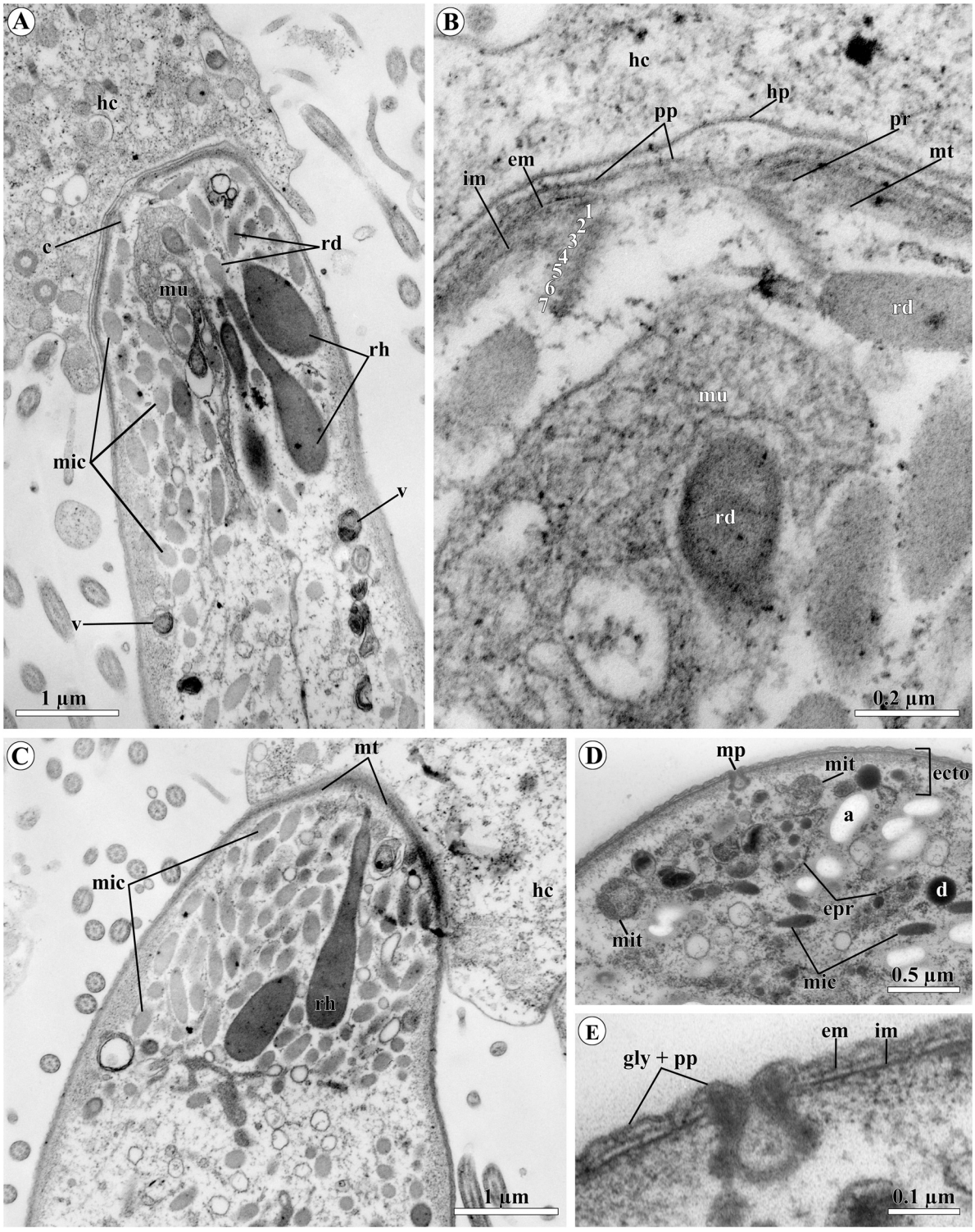

Figure 6. Fine structure of *Selenidium pherusae* sp. n. Transmission electron micrographs. **A**. Longitudinal section of the anterior end of a trophozoite. **B**. Detail of A showing the mucron structure. Numerals indicate the ordering numbers of the conoid microtubules. **C**. Superficial longitudinal section of the anterior end of another trophozoite. **D**. Transversal section of the anterior third of the trophozoite showing its cytoplasmic organization. **E**. Detail of D showing the micropore and pellicle structure. a, amylopectin granules; c, conoid; d,

pellicular microtubules arose from the polar ring and ran along the cell (Fig. 6B, C). A voluminous mucronal vacuole of irregular shape was present in the basal part of the conoid (Fig. 6A). It contained unidentified heterogeneous material and a few vesicles with electron-translucent content. The mucronal vacuole was surrounded by numerous rhoptries and micronemes. The ducts of the rhoptries extended to the apical pole of the parasite and closely adjoined the mucronal vacuole. The content of the ducts was less electron-dense than that of the rhoptries (Fig. 6A–C).

Numerous putative micronemes and several vesicles with an electron-dense material within multi-membranous whorls were present in the cytoplasm of the anterior third of the parasite (Fig. 6A). Similarly to *S. pygospionis*, the entire cytoplasm of *S. pherusae* trophozoites was indistinctly differentiated into the ectoplasm and the endoplasm, which had a similar content (Fig. 6D). In contrast to *S. pygospionis*, only a few mitochondria were observed near the pellicle, under subpellicular microtubules (Fig. 6D).

Molecular Phylogeny

Characteristics of DNA sequences: The contiguous sequence of *S. pygospionis* from *Pygospio elegans* (White Sea) was generated from four overlapping fragments and comprised SSU (small subunit or 18S), 5.8S, LSU (large subunit or 28S) rDNAs, and the internal transcribed spacers ITS 1 and 2 (4,910 bp totally). For *S. pygospionis* from *Polydora glycymerica* (Sea of Japan), only the near complete SSU rDNA sequence (1,610 bp) was obtained; it was nearly identical with that from the White Sea sample (only 2 substitutions). The contiguous sequence of *S. pherusae* (2,551 bp) was generated from two overlapping fragments and comprised SSU, 5.8S, the first ~600 nucleotides of the LSU rDNA, and the internal transcribed spacers ITS 1 and ITS 2 (Table 1 and Supplementary Material Fig. S1).

Phylogenies inferred from SSU rDNA: Both Bayesian inference (BI) and Maximum likelihood (ML) analyses resulted in similar tree topologies differing from each other by the position of platyproteids ("squirmids"): they were the earliest branch of Myzozoa in the Bayesian tree (Fig. 7), but the sister group of Apicomplexa in the ML tree (data not shown). Overall, the newly obtained phylogenies matched recent molecular phylogenetic evidence from alveolates and apicomplexans (e.g., Cavalier-Smith 2014; Janouškovec et al., 2015; Lepelletier et al. 2014; Rueckert and Horák 2017; Schrével et al. 2016). The resulting Bayesian tree inferred from the dataset of 128 taxa and 1,550 sites (Fig. 7) showed the monophyly of major alveolate groups, although chiefly with moderate or low support, especially in the ML analysis. The backbone of the apicomplexan region in the obtained trees was poorly resolved by both BI and ML analyses. Within the sporozoans (parasitic apicomplexans), the cryptosporidians were consistently located as the sister group of the "short-branching" eugregarine clade Eg1 (Actinocephaloidea and Stylocephaloidea) in both analyses, although with moderate Bayesian posterior probabilities (PP) and low ML bootstrap percentage (BP) supports. The top of the phylogenetic tree was formed by several long branches of eugregarines grouping into the loose clade Eg2 (Fig. 7); thus, eugregarines and, consequently, gregarines in general were not monophyletic, but polyphyletic.

Archigregarines branched after the cryptosporidians + Eg1 clade; they were not monophyletic either, being split into four firmly supported major lineages of greatly variable lengths (Ag1–Ag4), which arose successively from the backbone of the phylogenetic tree (Fig. 7). The earliest lineage Ag4 (PP = 0.99, BP = 40%) encompassed a robust clade comprising four parasites from polychaetes of the family Terebellidae and its sister group (PP = 99, BP = 62%) consisting of two environmental sequences. In contrast to the results obtained by Rueckert and Horák (2017), the archigregarine *Selenidium fallax* from the cirratulid polychaete *Cirriformia tentaculata* represented the isolated lineage Ag3 located not as sister to the cryptosporidia + gregarines clade but between the archigregarine clades Ag4 and Ag2 + Ag1 in the resulting phylogenies from both BI and ML analyses, though its nodal support was weak (Fig. 7). The robust lineages Ag2 and Ag1 formed a common clade, although weakly supported. This clade was located as a sister to the very weakly supported eugregarine clade Eg2

electron-dense droplet; ecto, ectocyte; em, external cytomembrane; epr, membranes of the rough endoplasmic reticulum; gly, glycocalyx; hc, host cell; hp, host cell plasmalemma; im, inner cytomembrane; mic, micronemes; mit, mitochondria; mp, micropore; mt, microtubules; mu, mucronal vacuole; pp, parasite plasmalemma; pr, polar ring; rd, ducts of rhoptries; rh, rhoptries; v, vesicles with multi-membrane whorls or dense material.

Table 1. Main characteristics of the archigregarine sequences obtained in this study.

Sample name, length of resulting sequence and its accession number	Amplified fragment	Length	Primers: forward (F) and reverse (R); annealing temperature used in the PCRs
Selenidium pygospionis from *Pygospio elegans* (White Sea) 4,910 bp MH061278	(I) SSU rDNA (part)	~1,640 bp	(F)[a] 5′-GTATCTGGTTGATCCTGCCAGT-3′ (R) 5′-GGAAACCTTGTTACGACTTCTC-3′ t° = 45 °C
	(II) SSU rDNA (part), ITS1, 5.8S rDNA, ITS2, LSU rDNA (part)	~1,110 bp	(F) 5′-CCGTTCTTAGTTGGTGG-3′ (R)[b] 5′-CRGTACTTGTBBDCTATCG-3′ t° = 45 °C
	(III) LSU rDNA (part)	~1,770 bp	(F)[b] 5′-ACCCGCTGAAYTTAAGCATAT-3′ (R)[b] 5′-GCCAATCCTTATCCCGAAGTTAC-3′ t° = 50 °C
	(IV) LSU rDNA (part)	~1,740 bp	(F)[b] 5′-TCCGCTAAGGAGTGTGTAACAAC-3′ (R)[b] 5′-TTCTGACTTAGAGGCGTTCAG-3′ t° = 50 °C
Selenidium pygospionis from *Polydora glycymerica* (Sea of Japan) 1,610 bp MH061279	(V) SSU rDNA (part)	~1,610 bp	(F)[a] 5′-GTATCTGGTTGATCCTGCCAGT-3′ (R) 5′-GGAAACCTTGTTACGACTTCTC-3′ t° = 45 °C
Selenidium pherusae 2,551 bp MH061280	(VI) SSU rDNA (part)	~1,600 bp	(F)[a] 5′-GTATCTGGTTGATCCTGCCAGT-3′ (R) 5′-GGAAACCTTGTTACGACTTCTC-3′ t° = 45 °C
	(VII) SSU rDNA (part), ITS1, 5.8S rDNA, ITS2, LSU rDNA (part)	~1,040 bp	(F)[b] 5′-TCCGCTAAGGAGTGTGTAACAAC-3′ (R)[b] 5′-CCTTGGTCCGTGTTTCAAGAC-3′ t° = 50 °C

[a]The primer sequence was based on Medlin et al., 1988.
[b]The primer sequences were based on Van der Auwera et al., 1994.

(see above), i.e. archigregarines were paraphyletic in the resulting SSU rDNA-based phylogenies; however, the nodal support of this grouping was low (Fig. 7). The archigregarine paraphyly has been repeatedly reported before but always with weak support (Rueckert and Horák 2017; Rueckert et al. 2011; Schrével et al. 2016; Wakeman et al. 2014; Wakeman and Horiguchi 2018; Wakeman and Leander 2013). Thus, the deep branching of archigregarine lineages had remained unresolved. Therefore, we tested alternative phylogenies (see below). The lineage Ag2 comprised two parasites of sipunculids and one environmental sequence.

The lineage Ag1 was the largest and comprised parasites of polychaetes from the families Cirratulidae, Flabelligeridae, Opheliidae, Sabellidae, Sabellariidae, Serpulidae, and Spionidae, including the newly obtained archigregarine sequences, and a number of environmental sequences, only two of which were involved in the final phylogenetic analyses. This was the longest archigregarine branch, which had full support in both BI and ML analyses. Number "1" was assigned to this clade because *Selenidium pendula*, the type species of the genus *Selenidium*, belonged to it (Fig. 7). Within the clade, the parasites of Serpulidae and Sabellariidae formed robust subclades, whilst the subclade of the parasites of Spionidae had full BP and moderate BP support. The two available sequences of the parasites of Sabellidae did not form a subclade, although they occupied neighbouring positions in the tree with moderate or low nodal supports; this indicates that their positions are actually unresolved. Both sequences of *S. pygospionis* (from *Pygospio elegans* and *Polydora glycymerica*) grouped with the sequences of *S. boccardiellae* and *S. pendula* within the subclade of parasites of spionid polychaetes (see above). The sequence of *S. pherusae* branched earlier, after *S. opheliae* from the polychaete *Ophelia roscoffensis* (Opheliidae); both these branches had moderate or low nodal supports.

Analyses of LSU rDNA and the ribosomal operon: All phylogenies based on these phylogenetic markers resulted in identical topologies both in the BI (Fig. 8) and the ML (not shown) analysis. Overall, they recovered the major alveolate clades that agreed with the phylogenies inferred from SSU rDNA, both already published (see above) and newly obtained, but with a higher resolution of all-alveolate and myzozoan deep branching.

Unlike SSU rDNA-based phylogenies, all analyses of the LSU rDNA dataset (53 sequences, 2,913 sites) resulted in the well-supported monophyly of gregarines (PP = 1.0, BP = 91). The only archigregarine sequence (*S. pygospionis* from *P. elegans*) formed a long branch (PP = 1.0, BP = 70) immediately after the clade Eg1 containing sequences of the "short-branching" gregarines *Ascogregarina taiwanensis* and Neogregarinida sp. OPPPC1 AB748927 and before the clade Eg2 including sequences of the "long-branching" eugregarines. Therefore, it broke down the monophyly of eugregarines (Fig. 8A).

The resulting phylogenetic trees inferred from the ribosomal operon dataset (alignment of 53 sequences, 4,618 sites) showed the same topology as the LSU rDNA-based phylogenetic tree with increased support for several branches (Fig. 8B). Within the sporozoan clade, all the studied gregarines were monophyletic, and the support was almost the same as in the LSU rDNA phylogenies. However, the BP support for the position of *S. pygospionis*, splitting eugregarine monophyly, was somewhat lower (BP = 64% vs 70% in the LSU rDNA tree).

Testing alternative phylogenies: Alternative topologies of phylogenetic trees were analyzed together with the topologies of the resulting tree yielded by the phylogenetic analyses (the reference tree, Fig. 7) with the use of the set of six widespread tests (see Methods). The results are presented in Figure 9 and Supplementary Material Table S1. For SSU rDNA phylogenies based on 128 sequences, the hypotheses on the monophyly of archigregarines and various positions of this combined lineage (Ag1 + Ag2 + Ag3 + Ag4) within the cryptosporidian-gregarine clade and sisterly to it were tested under the assumptions of monophyly or polyphyly of eugregarines (Fig. 9A). In addition to the resulting phylogenetic trees exhibiting the archigregarine paraphyly (see above), two of the four alternative SSU rDNA phylogenies containing monophyletic archigregarines were found not to be rejected by any test; this contradicts the results obtained by Rueckert and Horák (2017). Both these phylogenies included monophyletic eugregarines: (i) monophyletic archigregarines as a sister group either to monophyletic eugregarines (which means the monophyly of the gregarines as a whole) or (ii) to the clade comprising cryptosporidians and monophyletic eugregarines. All the tests rejected simultaneous monophyly of archigregarines and polyphyly of eugregarines (Fig. 9A and Supplementary Material Table S1).

For the LSU rDNA- and ribosomal operon-based phylogenies, the phylogenetic position of the only available archigregarine sequence, *S. pygospionis*

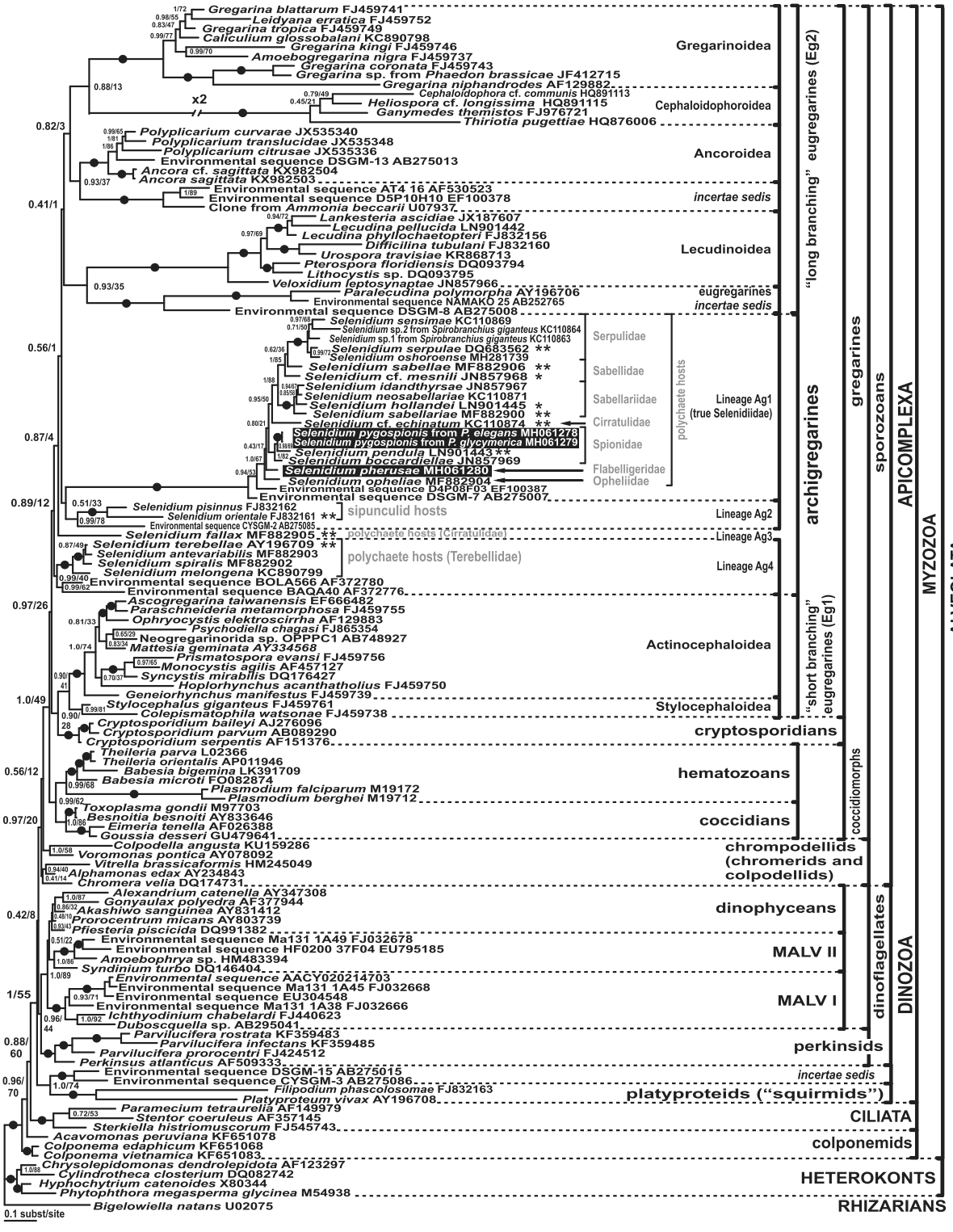

Figure 7. Bayesian inference tree of alveolates inferred from the dataset of 128 SSU rDNA sequences and 1,550 sites under the GTR + Γ + I model. Numbers at the nodes indicate Bayesian posterior probabilities (numerator) and ML bootstrap percentage (denominator). Black dots on the branches indicate Bayesian posterior probabilities and bootstrap percentages of 0.95 and 90% or more, respectively. The newly obtained sequences

from *P. elegans*, was examined, and the same set of topologies was used (Fig. 9B and C, and Supplementary Material Table S1). Congruently to SSU rDNA-based phylogenies, the hypothesis of its sister position to monophyletic eugregarines was not rejected by any test among the phylogenies based both on LSU rDNA (Fig. 9B) and on the ribosomal operon (Fig. 9C). All the other topologies were rejected by all tests among LSU rDNA-based phylogenies but among operon-based phylogenies the polyphyly of eugregarines was not rejected in the case when the archigregarine was a sister lineage to the eugregarine clade Eg2 and cryptosporidians were a sister group to the clade Eg1, i.e. as in the SSU rDNA reference tree.

Summing up, the monophyletic archigregarines as a sister group to the monophyletic eugregarines was the only possible alternative topology (permitted by all the tests) shared by the phylogenies based on all the three genetic markers used (SSU rDNA, LSU rDNA, and ribosomal operon phylogenies). However, the number of sequences in the LSU rDNA/ribosomal operon database is significantly lower than in the SSU rDNA database and is still insufficient to make valid comparisons and meaningful conclusions.

Discussion

Justification of Newly Described Species

Selenidium pygospionis sp. n.

There are currently eleven species of archigregarines inhabiting polychaetes of the family Spionidae (Dibb 1938; de Faria et al. 1917; Fowell 1936a,b; Ganapati 1946; Giard 1884; Levine 1971; Ray 1930; Reichenow 1932; Wakeman and Leander 2012). They are described in varying degree of detail; in particular, only three species have been examined by electron microscopy: *Selenidium pendula*, *S. boccardiellae*, and *S. pygospionis sp. n.* (Rueckert and Horák 2017; Schrével et al. 2016; Wakeman and Leander 2012; this study). Most of these archigregarines belong to the genus *Selenidium*, one archigregarine belongs to the genus *Selenocystis* (*S. foliata*). However, *Selenidium foliatum* Ray, 1930 is suggested to be a synonym of *S. foliata* Dibb, 1938 (Desportes and Schrével 2013; Dibb 1938; Schrével 1970). We also suspect that *Selenidium intraepitheliale* Reichenow, 1932 may be a synonym of *S. spionis* (Kolliker, 1945) Ray, 1930 as these archigregarines parasitizing the same host are identical (Levine 1971; Ray 1930; Reichenow 1932; Schrével 1970). The resulting combinations of archigregarines from spionid polychaetes are presented in Supplementary Material Table S2. Additionally, three *Selenidium* species were reported from the spionid polychaetes *Dipolydora coeca* (Caullery and Mesnil 1899), *Spio filicornis* (Caullery and Mesnil 1901), and *Pygospio elegans* (Caullery and Mesnil 1899; Reichenow 1932) without species descriptions.

The archigregarines from spionids are usually characterized by a high frequency and a middle intensity of parasite infection (Douglass and Jones 1991). Merogony was reliably shown only in *S. axiferens* (Fowell 1936b). At the same time, the presence of numerous individuals of an archigregarine in a spionid polychaete was considered as an indirect evidence of the presence of merogony in their life cycle (Schrével et al. 2016). They usually have a vermiform, more or less flattened cell, with a knob-shaped (dome-shaped) mucron. Some of them, including the type species *S. pendula*, have an optically distinct cytoplasm arranged along the cell axis, around the nucleus and in the radials running to the cell periphery (Desportes and Schrével 2013; Fowell 1936a,b; Ray 1930; Rueckert and Horák 2017).

Trophozoites of *Selenidium pygospionis* sp. n. isolated from *Pygospio elegans* polychaetes in this study were somewhat similar with *S. spionis*, *S. intraepitheliale*, *S. martinensis*, parasitizing in various hosts, in cell size, cell shape, and in the number of longitudinal folds (Levine 1971; Ray 1930; Reichenow 1932; Supplementary Material Table S2). However, the trophozoites of *S. pygospionis* were easy to distinguish from other species of *Selenidium* by their hook-like anterior end. Therefore, we established a new species for these archigregarines using host-specific and morphological characteristics as well as molecular-phylogenetic markers.

The molecular-phylogenetic analyses revealed an almost full identity (two substitutions per 1,610 bp) of sequences from archigregarines isolated from the polychaetes *P. elegans* of the

of *Selenidium* spp. are highlighted by black. Single asterisks indicate "*Selenidioides*" spp. and double asterisks – "*Selenidium*" spp. as proposed in the revision by Levine (1971). The information about the host taxonomical affiliations is given in gray.

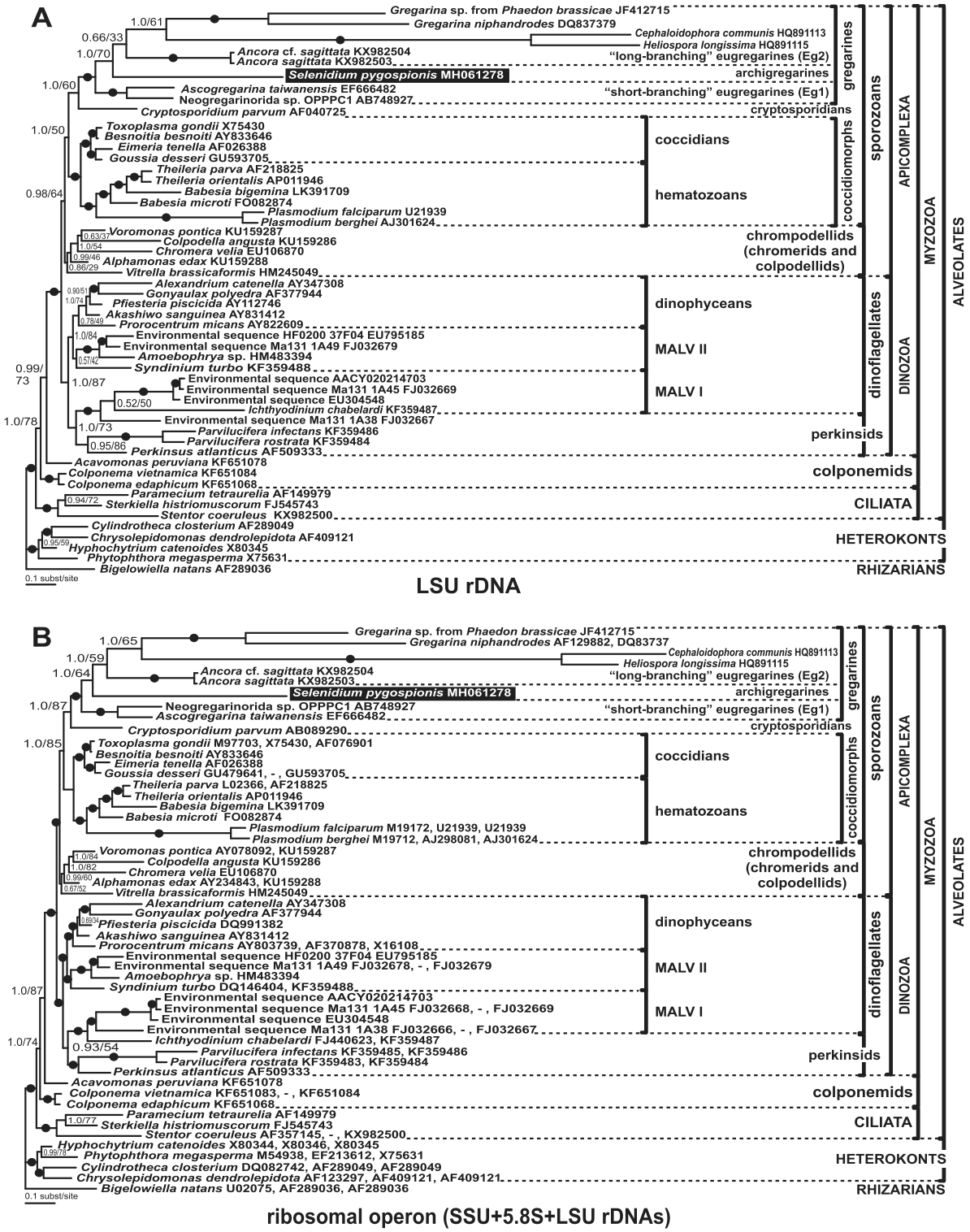

Figure 8. Bayesian inference trees of alveolates inferred from the datasets of 53 taxa under GTR + Γ + I model for, **A**, LSU rDNA (2,913-sites dataset); **B**, ribosomal operon (4,618-sites dataset). Numbers at the nodes indicate Bayesian posterior probabilities (numerator) and ML bootstrap percentage (denominator). Black dots on the branches indicate Bayesian posterior probabilities and bootstrap percentages of 0.95 and 90% or more,

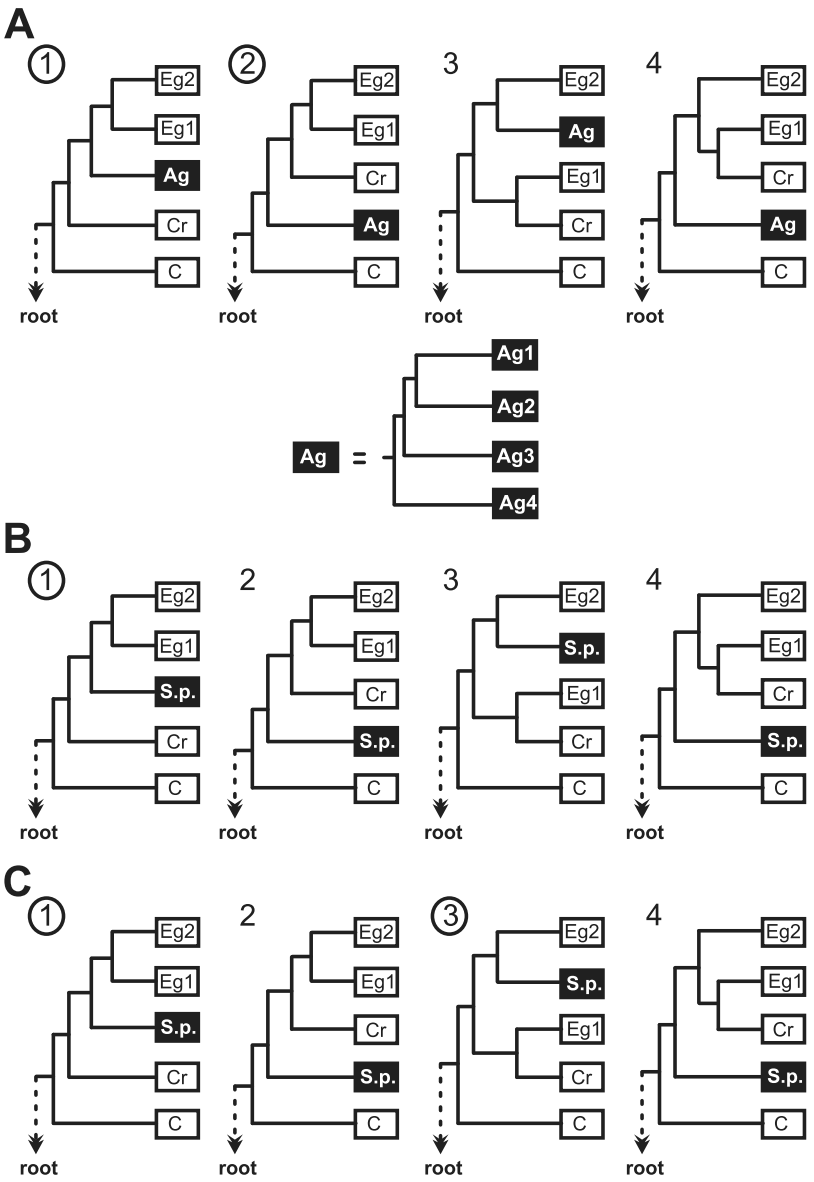

Figure 9. Tested alternative topologies of phylogenetic trees. **A**, testing archigregarine monophyly on alternative topologies for the SSU rDNA phylogenies (the dataset of 128 taxa and 1,550 sites). The scheme below the raw of the alternative topologies shows the structure of the artificially composed monophyletic archigregarine clade. **B** and **C**, testing phylogenetic position of the archigregarine *Selenidium pygospionis* from *Pygospio elegans* on alternative topologies for the (**B**) LSU rDNA phylogenies (the dataset of 53 taxa and 2,913 sites) and (**C)** ribosomal operon phylogenies (the dataset of 53 taxa and 4,618 sites). Permissible topologies (not discarded by all tests) are marked by numbers within circles. Abbreviations: **Ag1**, archigregarines (the subclade numbers in the scheme correspond those in Fig. 8); **Eg1** and **2**, eugregarine clades (short- and long-branching, respectively; see Figs 8 and 9); **Cr**, cryptosporidia; **C**, coccidiomorphs (Coccidia and Hematozoa); **S.p.**, the sequences of *S. pygospionis*.

respectively. The newly obtained sequences of the archigregarine *Selenidium pygospionis* is highlighted by black. Accession numbers in the tree **B** are arranged in following order: SSU rDNA, 5.8S (if not available then "–"), LSU rDNA.

White Sea and *Polydora glycymerica* of the Sea of Japan. This means that these archigregarines, though isolated from hosts from geographically distinct regions, belong to the same species, *S. pygospionis*. We also suspect that *Selenidium* sp. from *P. elegans* (former *P. seticornis*) collected near Plymouth, the English Channel (Caullery and Mesnil 1899; Reichenow 1932), is *S. pygospionis* described in the present study. These data indicate that the biogeographic distribution of archigregarines may be extensive and that the systematic principle "new host – new species", sometimes used for gregarines (Levine 1971), should be applied to archigregarines with caution.

We believe that the archigregarine recently found to harbor the microsporidium *Metchnikovella dogieli* (Paskerova et al. 2016) is likely to be *S. pygospionis* since it had been sampled at the same site where samples for the present study were taken. Metchnikovellidean microsporidia, inhabiting both archigregarines and eugregarines (Desportes and Schrével 2013; Mikhailov et al. 2017; Rotari et al. 2015; Sokolova et al. 2013, 2014), appear to possess a universal complex of adaptations (mechanisms of invasion, life cycles, metabolic strategies, etc.) allowing them to parasitize in structurally different gregarines.

Selenidium pherusae sp. n.

Only four archigregarine species have been known to parasitize polychaetes of the family Flabelligeridae (Bogolepova 1953; Castellon and Gracia 1988; Kuvardina and Simdyanov 2002; Simdyanov 1992; Tuzet and Ormières 1958; Tuzet and Ormières 1965). The resulting combinations of archigregarines from flabelligerid polychaetes are presented in Supplementary Material Table S3. All of them belong to the genus *Selenidium*, and almost all have a longitudinally folded cortex, except *S. pennatum* which has two lateral vanes or ridges (Simdyanov 1992). Only one archigregarine species has been described from the polychaete *Pherusa plumosa*, *S. curvicollum* (Bogolepova 1953). Its trophozoites have 13–15 cortical grooves per side and a large, curved proboscis-like anterior end. The archigregarine described in the present study parasitizes the intestine of the polychaete *Ph. plumosa*; however, it lacks any folds at the surface and has a small, slightly truncated mucron. Hence, we consider it as a new species, *Selenidium pherusae* sp. n.

Nutrition of Archigregarines

Myzocytotic feeding (myzocytosis), i.e. sucking the host cell cytoplasm via a well-developed apical complex, was found in *S. hollandei*, *S. pendula* and *S. orientale* (Schrével 1968, 1971b; Schrével et al. 2016; Simdyanov and Kuvardina 2007). It is thought that myzocytosis is common in archigregarines (Desportes and Schrével 2013; Schrével et al. 2016; Simdyanov and Kuvardina 2007; Wakeman and Horiguchi 2018; Wakeman et al. 2014). In the mucron of *S. pygospionis* and *S. pherusae*, we observed the organelles of the apical complex such as the conoid, the mucronal vacuole, rhoptries, and micronemes. Additionally, a series of connected vacuoles arranged along the cell axis and around the nucleus was present in *S. pygospionis*. We suggest that the axial streak of *S. pygospionis*, well visible in living archigregarines under a light microscope, is a system of the observed (presumably digestive) vacuoles originating in the mucron during the myzocytosis and transporting nutrients from the anterior to the posterior end along the cell axis. To note, numerous vacuoles around the nucleus have also been found in the cytoplasm of *S. pendula* (Schrével 1970, 1971a). These vacuoles may be a component of a similar system of digestive vacuoles.

Different cytoplasmic vesicles containing some multi-membranous whorls or dense material and located in the ectoplasm near the pellicle or inserted in the inner membrane complex were previously observed in several *Selenidium* spp. (Schrével 1971a; Schrével et al. 2016; Wakeman and Horiguchi 2018). It was suggested that these structures might be involved in a surface-mediated nutrition present alongside with the nutrition via the typically organized micropores (Wakeman and Horiguchi 2018).

The heterogeneity of the organelles' distribution (narrow electron-translucent spaces lacking any visible organelles) observed in the cytoplasm of *S. pygospionis* may point to the presence of microfilaments similar to those demonstrated around the nucleus in *S. pendula* and *S. hollandei* (Schrével 1971a). Putative digestive vacuoles and coexisting microfilaments may play a role in the transport of nutrients from the anterior to posterior end during myzocytotic feeding.

Motility of Archigregarines

In general, archigregarines show different types of movement such as bending, twisting, coiling, rolling, and pendular motility. Some of them can also contract their cell. These movements were often likened to those of nematode worms (Fowell 1936a,b; Gunderson and Small 1986; Leander 2007, 2008b; Mellor and Stebbings 1980; Schrével 1971a,b; Schrével et al. 1974, 2016; Stebbings et al. 1974; Wakeman et al. 2014). Both archigregarines described in the present study can move by forming 1–4 (in *S. pygospionis*) or only one (in *S. pherusae*) bending sections along the cell but never contract. Additionally, as it can be easily seen in flattened trophozoites of *S. pygospionis*, their bending motility is generated only in one cell plane. We propose to refer to this type of motility as a nematode-like bending, where the alternate sides (flattened sides in *S. pygospionis* or body halves in *S. pherusae*) act antagonistically in the bending sections forming in a single plane of the cell. It is similar to the pendular motility of *S. pendula*, where one bend is generated in the anterior part of the cell and runs to the posterior one, but considerably different from the bending motility of other *Selenidium* spp. (e.g. *S. hollandei*, *S. sabellariae*), where bends, generated in different cell planes, can combine with contraction and twisting of the cell in different cell sections (Desportes and Schrével 2013; Rueckert and Horák 2017; Schrével 1967, 1970). The character of archigregarine motility may reflect the dynamics and architecture of the cytoskeleton.

Nematode-like bending is an evidence in favour of the general hypothesis about motility of *Selenidium* spp. postulating that the three-membrane pellicle and the longitudinal microtubules are skeletal and motile units representing together a unicellular analogue of the musculocuticular system of nematodes (Leander 2007, 2008b; Stebbings et al. 1974). A similar motility mechanism was also demonstrated in the blastogregarine *Siedleckia nematoides.* It performs pendular, twisting, undulating movements and possesses the longitudinal microtubules organized in a layer or layers under the trimembrane pellicle (Valigurová et al. 2017). To note, the axial streak together with putative microfilaments may also be involved in the cell motility as an additional skeletal element helping to reverse movement and maintenance of the cell shape in bends as suggested by the concept of the statomotor system (Fowell 1936b).

According to the previous authors, the dynamic motility of archigregarines and blastogregarines is correlated with the number of mitochondria located directly beneath the subpellicular microtubules (Desportes and Schrével 2013; Leander 2006, 2007; Mellor and Stebbings 1980; Schrével 1971b; Stebbings et al. 1974; Valigurová et al. 2017). Our observations of the ultrastructure of both studied archigregarines may lend further support to this idea. An actively bending (up to 4 bends at a time) *S. pygospionis* has numerous mitochondria arranged in a layer beneath the subpellicular microtubules, while a less pronouncedly bending (only one bend at a time) *S. pherusae* has fewer mitochondria.

Intracellular Development in *Selenidium pygospionis* sp. n.

We observed small cells of putative *S. pygospionis* localized within the parasitophorous vacuoles in the host enterocytes. Intracellular young trophozoites were also found in other archigregarines such as *Selenidium spionis*, *S. mesnili*, *S. foliatum*, and *S. cauleryi* (Ray 1930). An intracellular localization may be an initial stage of the trophozoite development in some archigregarines. As trophozoites grow, the host cells are destroyed, and the location of the parasites becomes extracellular. In the case of *S. pygospionis*, well-developed and extracellularly localized trophozoites are anchored between the host intestinal epithelium folds by their hook-like anterior end. We do not know whether they form any attachment site with the host cell at some period of their development. Intra-tissue stages mentioned in the description of *S. spionis* and *S. foliatum* (Caullery and Mesnil 1899, 1901; Ray 1930) as a few full-grown individuals embedded in the intestine wall tissue under the epithelial layer and lying parallel to the host longitudinal axis can be regarded as an abnormal and occasional development of trophozoites.

Notes on the Taxonomy and Phylogeny of Archigregarines

Levine (1971) proposed to divide the genus *Selenidium* into two genera based on the presence/absence of merogony in the life cycle. He established a new genus, *Selenidioides*, for gregarines with merogony and assigned it to the archigregarines. The species without merogony (or in which merogony was unknown) were transferred to the eugregarines within the genus *Selenidium*.

In his opinion (Levine 1971), the data on ultrastructure and life cycles of archi- and eugregarines available at that time (MacGregor and Thomasson 1965; Schrével 1966, 1970, 1971a,b; Vávra 1969; Vivier and Schrével 1964, 1966; Vivier et al. 1970; etc.) were insufficient for the separation of these two groups. Levine's classification has become popular and has been applied in some revisions on protists and taxonomic databases (Perkins et al. 2000; WoRMS).

Available molecular phylogenetic evidence (Rueckert and Horák 2017; Rueckert and Leander 2009; Schrével et al. 2016; Wakeman and Horiguchi 2018; Wakeman and Leander 2012, 2013; Wakeman et al. 2014) and the results of this study show that the archigregarines are separated into several phylogenetic lineages. However, this separation does not correspond to the taxonomical action proposed by Levine. On one hand, the type species of the genus *Selenidium*, *S. pendula*, belong to the clade Ag1 ("true Selenidiidae" as proposed by Schrével et al. (2016)) together with representatives of the "*Selenidioides*" group, *S. mesnili* and *S. hollandei*. On the other hand, some gregarines of the "*Selenidium*" group, *S. terebellae*, *S. fallax*, and *S. orientale*, belong to the clades Ag2, Ag3, and Ag4 respectively, not to the clade Ag1 (Fig. 7). Thus, the taxonomical approach proposed by Levine (1971) for archigregarines should be abolished together with the genus *Selenidioides* Levine, 1971 as has already been suggested by different authors (Rueckert and Horák 2017; Rueckert and Leander 2009; Schrével et al. 2016; Wakeman and Leander 2012).

Overall, the molecular phylogeny of the archigregarines based on the available DNA sequences is largely congruent with the taxonomical affiliations of their hosts (Schrével et al. 2016; this study). Indeed, archigregarines of the lineage Ag4 inhabit polychaetes of the family Terebellidae, archigregarines of the lineage Ag2 occur in sipunculid hosts, while most *Selenidium* spp. of the lineage Ag1 parasitize in different sedentary polychaetes (Fig. 7), however, their grouping in subclades within this clade also agrees well with the taxonomical affiliations (families) of hosts. We consider that this reflects in various degrees some aspects of host-parasite coevolution, which may become an important subject of research in the future.

The macrosystem of archigregarines is questionable because of the issue of their monophyly, unresolved both in terms of the molecular phylogeny and the classic cladistic approach based on morphology. The morphology-based hypothesis about the monophyly of *Selenium*-like archigregarines is difficult to substantiate in terms of cladistics, as all their ultrastructural key features (the ultrastructure of the cortex and mucron) appear to be symplesiomorphies (the aforementioned morphostasis) rather than synapomorphies. Apart from *Selenidium* spp., morphologically different representatives of the genera *Ditrypanocystis*, *Exoschizon*, *Merogregarina*, *Meroselenidium*, and *Selenocystis* have also been affiliated to archigregarines (Desportes and Schrével 2013; Perkins et al. 2000). They are intestinal parasites of polychaetes and sipunculids as well as of colonial ascidians and oligochaetes. No molecular phylogenetic evidence from these parasites is currently available (Desportes and Schrével 2013) and electron-microscopic data are extremely scanty (Butaeva et al. 2006). Some of these organisms may be neither archigregarines nor even gregarines. A demonstrative example is the case of *Platyproteum* (formerly *Selenidium*) *vivax* and *Filipodium fascolosomae*, gregarine-like organisms, which have been shown to be an independent lineage of Myzozoa, so-called "squirmids" (Cavalier-Smith 2014; Rueckert and Leander 2009). Both parasites are capable of very dynamic cellular deformations referred to as the peristaltic motility (metaboly) (Gunderson and Small 1986; Leander 2006; Rueckert and Leander 2009). Since this is dissimilar to the real squirming, we prefer to call this lineage "platyproteids" (Fig. 7) instead of "squirmids" proposed by Cavalier-Smith (2014).

The SSU rDNA-based phylogenies (Cavalier-Smith 2014; Cavalier-Smith and Chao 2004; Grassé 1953; Rueckert and Leander 2009; Rueckert and Horák 2017; Schrével et al. 2016; Wakeman and Horiguchi 2018; Wakeman and Leander 2012, 2013; Wakeman et al. 2014; this study) reveal archigregarines as a paraphyletic group, although their deep branching is actually unresolved and shows weak nodal supports. The test of alternative topologies, provided in this study, did not reject archigregarine monophyly, but only within the framework of the hypothesis that eugregarines were monophyletic too (Fig. 9A). Thus, the phylogenetic analyses of the SSU rDNA yield ambiguous results. As explained previously (Simdyanov et al. 2017), SSU rDNA-based phylogenies appear to be of little use for resolving the deep branching order of gregarines and apicomplexans altogether. This is likely a consequence of an explosive evolutionary radiation of gregarines and/or rapid evolution of their SSU rDNA sequences. The LSU rDNA and near-complete rDNA operon provide an increased phylogenetic resolution over SSU rDNA and could be useful in

advancing the phylogeny and taxonomy of archigregarines and gregarines in general (Simdyanov et al. 2015, 2017). Unfortunately, only one archigregarine LSU rDNA sequence is now available (this study), and it even forms a long branch, so that its position in the obtained phylogenies might be affected by the long branch attraction artifact. An enhanced taxon sampling of archigregarine LSU rDNA sequences is necessary for more substantial conclusions, with special attention to short-branching species, representatives of the lineages Ag2, Ag3, and Ag4. Multigenic phylogenies including a broad representative sampling of archigregarines could provide the ultimate test of the hypotheses about the evolution within Apicomplexa.

Taxonomic Summary

Phylum Apicomplexa Levine, 1970

Subphylum Sporozoa Leuckart, 1879

Class Gregarinomorpha Grassé, 1953, emend. Simdyanov et al., 2017

Order Archigregarinida Grassé, 1953

Family Selenidiidae Brasil, 1907

Genus *Selenidium* Giard, 1884

Selenidium pygospionis sp. n.

Diagnosis. Trophozoites aseptate, elongated and slightly flattened with narrowed ends, embedded in the host intestinal epithelium (extracellular or intracellular location) or freely localized in the intestinal lumen. Anterior end usually hook-like, bent towards one of the wide sides. Mucron naked, dome-shaped. Trophozoites measuring 34 to 288 μm (average 144 μm, mode 146 μm, n = 79) in length, 4 to 25 μm (average 12 μm, mode 11 μm, n = 76) in width. Cell surface with 22–30 (usually 28, n = 12) broad and low folds separated by grooves. 10–12 grooves per flattened side and 1–3 grooves per narrow side. Nucleus oval, 6–22 μm (av. 17 μm, n = 40) × 5–11 μm (av. 8.4 μm, n = 26), located in the widest part and expanding along the longitudinal axis of the cell. Single nucleolus situated in nucleus part facing anterior end. Intracellular axial streak of optically distinct cytoplasm expanding from anterior to posterior end and forming expansion around nucleus and numerous radial threads toward cell periphery. Syzygy caudo-caudal. Attached or non-attached trophozoites and syzygy partners moving by nematode-like bending (formation of bends in a single plane of cell).

DNA sequences. SSU, ITS1, 5.8 S, ITS2, and LSU rDNA sequences for individuals, isolated from the polychaetes *Pygospio elegans* (White Sea) (GenBank MH061278) and SSU rDNA – from the polychaetes *Polydora glycymerica* (Sea of Japan) (GenBank MH061279).

Type material (syntypes). Resin blocks and fixed slides containing archigregarines and pieces of infected host intestine deposited in the collection of Department of Invertebrate Zoology, St Petersburg State University; Figures 1–4 (this publication) show some of the syntypes.

Hosts and localities. Polychaetes *Pygospio elegans* Claparède, 1863 (Spionidae, Polychaeta); Bolshoy Goreliy Island, Keret' Archipelago, Chupa Inlet, Kandalaksha Bay, White Sea, 66°18.770′N; 33°37.715′E; Velikaja Salma, Kandalaksha Bay, White Sea, 66°33.200′N, 33°6.283′E. Polychaetes *Polydora glycymerica* Radashevsky, 1993 (Spionidae, Polychaeta); Peter the Great Bay, Sea of Japan, 42°53′29″N, 132°44′07″E.

Location within host. Intestine (midgut and hindgut).

Etymology. Species name, *pygospionis*, refers to the genus name of one of the hosts.

Selenidium pherusae sp. n.

Diagnosis. Trophozoites aseptate, vermiform. Anterior end narrowed, slightly truncated; posterior end pointed in young or rounded in mature individuals. Cell surface smooth, without well-developed folds or grooves. Trophozoites measuring 38–269 μm (n = 6) in length, 10–18 μm (n = 4) in width. Nucleus spherical (11–12 μm, n = 2), located in the widest part of the posterior half of the cell, with the single nucleolus. Attached and detached trophozoites exhibiting bending motility.

DNA sequences. SSU rDNA sequences (GenBank MH061278).

Type material (syntypes). Resin blocks and fixed slides containing archigregarines and pieces of infected host intestine deposited in the collection of the author TGS, Department of Invertebrate Zoology, Lomonosov Moscow State University; Figures 5–6 (this publication) show some of the syntypes.

Host and locality. Polychaetes *Pherusa plumosa* (Müller, 1776) (Flabelligeridae, Polychaeta); Peter the Great Bay, Sea of Japan, 42°53′29″N, 132°44′07″E.

Location within host. Midgut.

Etymology. The species name, *pherusae*, refers to the genus name of the host.

Methods

Collection of polychaete hosts and isolation of gregarines: Polychaetes *Pygospio elegans* Claparède, 1863 (Spionidae, Polychaeta) were collected at two sites of the littoral zone near the Marine Biological Station of St Petersburg State University (Bolshoy Goreliy Island, Keret' Archipelago, Chupa Inlet, Kandalaksha Bay, White Sea, 66°18.770′N; 33°37.715′E) and the White Sea Biological Station of Lomonosov Moscow State University (Velikaja Salma, Kandalaksha Bay, White Sea, 66°33.200′N, 33°6.283′E) during the summers of 2002–2015 years.

Polychaetes *Polydora glycymerica* Radashevsky, 1993 (Spionidae, Polychaeta) boring shell walls of the living bivalves *Glycymeris yessoensis* (G. B. Sowerby III, 1889) and polychaetes *Pherusa plumosa* (Müller, 1776) (Flabelligeridae, Polychaeta) inhabiting druses of the Far East mussels *Crenomytilus grayanus* (Dunker, 1853) were collected by SCUBA divers in 2007 near Vostok biological station, National Scientific Center of Marine Biology, Russian Academy of Sciences (Peter the Great Bay, Sea of Japan, near Nakhodka, 42°53′29″N, 132°44′07″E).

Prior to dissection, the examined animals were stored in small containers (about 50 worms per 250 ml container) at +10 °C with periodically changed seawater. The polychaetes were cultured up to a month. Dissection of polychaetes and isolation of parasites were performed with the help of fine needles and hand-drawn glass pipettes under a stereomicroscope (MBS-10, Russia). The released parasites or small fragments of the host intestine with attached gregarines were rinsed thrice with seawater filtered through Millipore (0.22 μm), then prepared for light microscopy or fixed for electron microscopy. Individual cells were also subjected to DNA extraction.

Light microscopy: More than 100 polychaetes of *P. elegans* were investigated in squash preparations [compressing of a polychaete specimen between the object and cover slides before microscopic analysis] (Fig. 1A–B, D–M). Separate archigregarines isolated from the intestines of *P. elegans* (Fig. 1C, N–Q), *P. glycymerica* (data not shown) and *Ph. plumosa* (Fig. 5A) were also investigated in living preparations. All preparations were investigated with the use of a series of light microscopes equipped with different digital cameras: a MBR-1 microscope (LOMO, Russia) equipped with phase contrast and connected to a Canon EOS 300D digital camera; a Zeiss microscope (Carl Zeiss, Germany) connected to a Nikon Coolpix 7900 camera; a Zeiss Axio Imager.A1 connected to an AxioCam MRc5 digital camera (Carl Zeiss, Germany); a Leica DM 2500 microscope equipped with DIC optics and Plan-Apo objective lenses and connected to a DFC 295 digital camera (Leica, Germany).

Several individuals of *S. pherusae* from polychaetes *Ph. plumosa* were fixed with 3% formaldehyde in seawater, stained with Carazzi's hematoxylin and examined under a Zeiss microscope connected to a Nikon Coolpix 7900 camera (Fig. 5B).

Electron microscopy: Small pieces of the polychaete intestine with attached archigregarines or free archigregarines released from the host gut lumen were fixed in 2.5% glutaraldehyde in 0.2 M cacodylate buffer with/without 0.05% MgCl2 (pH 7.4, final osmolarity 720 mOsm) for 1–4 h, washed in filtered seawater and postfixed in 1–2% osmium tetroxide in the same buffer for 1–2 h. The entire procedure of fixation was performed at +4 °C. Fixed samples were dehydrated in an ascending ethanol series. Some of them were additionally transferred to an ethanol/acetone mixture and rinsed in pure acetone before the following procedure. For SEM, the fixed and dehydrated samples were critical point dried in liquid CO_2 and then coated with gold or platinum. The samples were investigated with a Tescan MIRA3 LMU scanning electron microscope (TESCAN Brno, Czech Republic), JSM-7401F (JEOL, Japan), FEI Quanta 250 (Thermo Fisher Scientific, Netherlands) and Hitachi S-405A scanning electron microscope (Hitachi, Japan) (Figs 2, 5C, D). For TEM, fixed and dehydrated samples were embedded in Epon-Araldite or Epon blocks. They were sectioned with ultramicrotomes Leica EM UC6 and Leica EM UC7 (Leica, Germany). Ultra-thin sections were stained according to standard protocols (Reynolds, 1963) and examined using a JEM 2100 (JEOL, Japan), TEM–1010 (JEOL, Japan), and LEO 910 (Carl Zeiss, Germany) electron microscopes equipped with a digital or film cameras. In total, more than 20 gregarines from *P. elegans* (Figs 3, 4A–C, F, G), about five gregarines from *P. glycymerica* (data not shown) and five gregarines from *Ph. plumosa* (Fig. 6) were sectioned and examined by TEM.

Ten entire worms of *P. elegans* were fixed in Bouin's solution. The material was dehydrated in a graded alcohol series, infiltrated in a graded series of chloroform-Histomix and finally embedded in Histomix paraffin wax (BioVitrum, Russian Federation). Serial sagittal or coronal sections were prepared on a Microm HM 360 rotary microtome (0.1–1 mm in thick). Sections were mounted on the object slides. The preparations were deparaffinized in xylol and then washed in acetone. After critical point drying in liquid CO_2 and coating with gold, they were observed under a Tescan MIRA3 LMU scanning electron microscope (TESCAN Brno, Czech Republic) (Fig. 4D, E).

DNA isolation, PCR and sequencing: Trophozoites of the gregarine *Selenidium pygospionis*, about 100 cells isolated from the polychaete *P. elegans* (Bolshoy Goreliy Island, Kandalaksha Bay, White Sea, 2009), were fixed and stored in RNAlater stabilization solution (Life Technologies, USA). DNA extraction of this sample was performed with the Diatom DNA Prep 200 kit (Isogen, Russia). About ten trophozoites and one syzygy of *S. pygospionis* isolated from polychaetes *P. glycymerica* (Peter the Great Bay, Sea of Japan, 2007) were rinsed with seawater, deposited into 1.5-ml microcentrifuge tubes and then were lyzed by the alkaline procedure (Floyd et al. 2002). In a similar manner, 25 trophozoites of the gregarine *S. pherusae* isolated from polychaete *Ph. plumosa* (Peter the Great Bay, Sea of Japan, 2007) were lysed. The lysates obtained in two last cases were directly used in PCR.

The nucleotide sequences of *S. pygospionis* from *P. elegans* and *S. pherusae* were amplified in several PCRs with different pairs of primers (Table 1 and Supplementary Material Fig. S1). A set of overlapping fragments (I–IV and VI–VII, respectively; see Supplementary Material Fig. S1) encompassing SSU rDNA, ITS 1 and 2, 5.8S rDNA, and LSU rDNA was obtained. For *S. pygospionis* from *P. glycymerica*, only one fragment (V) containing the near complete SSU rDNA was PCR-amplified (Table 1 and Supplementary Material Fig. S1). All PCRs were performed with an Encyclo PCR kit (Evrogen, Russia) in a total

volume of 25 μl using a DNA Engine Dyad thermocycler (Bio-Rad) and the following protocol: initial denaturation at 95 °C for 3 min; 40 cycles of 95 °C for 30 sec, annealing at 45 °C (fragments I, II, V, and VI) or 50 °C (fragments III, IV, and VII) for 30 sec, and extension at 72 °C for 1.5 min; and final extension at 72 °C for 10 min. PCR products of the expected size were gel-isolated by a Cytokine DNA isolation kit (Cytokine, Russia). For fragments I, II, and IV–VII, the PCR products were sequenced directly. Fragment III was cloned by using an InsTAclone PCR Cloning Kit (Fermentas, Lithuania) because the corresponding PCR product was heterogeneous. Sequences were obtained by using an ABI PRISM BigDye Terminator v. 3.1 reagent kit and an Applied Biosystems 3730 DNA Analyzer for automatic sequencing. After assembling the read fragments with the use of the BioEdit 7.0.9.0 program (Hall 1999), the resulting contiguous sequences were deposited in GenBank (accession numbers: MH061278–80).

Molecular phylogenetic analysis: Four nucleotide alignments were prepared for phylogenetic analyses: SSU (18S) rDNA (128 and 53 sequences), LSU (28S) rDNA, and ribosome operon (concatenated SSU, 5.8S, and LSU rDNA sequences). The alignments were generated in the MUSCLE 3.6 program (Edgar 2004) and manually adjusted with the use of the BioEdit 7.0.9.0 program (Hall 1999): gaps, columns containing few nucleotides and hypervariable regions were removed. The final length of the alignments was 1,550 bp. The taxon sampling of 128 sequences alignment was designed as to maximize the phylogenetic diversity and the completeness of sequences in the alignments. Representatives of heterokonts and rhizarians were used as outgroups. The "reduced" SSU rDNA alignment (53 sequences, 1,550 sites) was used as a constituent part of the concatenated ribosomal operon dataset and, consequently, covered the same taxon sampling.

For the LSU rDNA and ribosomal operon (concatenated SSU, 5.8S, and LSU rDNAs) analyses, taxon sampling of only 53 sequences were used due to the limited availability of data for LSU rDNA and, especially, 5.8S rDNA. Therefore, the 5.8S rDNA (155 sites in the alignment) was rejected from the analysis of concatenated rDNA genes for seven sequences (*Chromera velia*, *Colponema vietnamica*, *Goussia desseri*, *Stentor coeruleus*, and 3 environmental sequences: Ma131 1A38, Ma131 1A45, and Ma131 1A49): the corresponding 155 positions were replaced with "N" in the final ribosomal operon dataset. The resulting datasets contained 53 sequences (2,913 sites) for the LSU rDNA and the concatenated rDNA sequences (4,618 sites) of the same 53 taxa for the ribosomal operon. Thus, both taxon samplings comprised an identical set of species, all of which were also represented in the alignment of the 128 SSU rDNA sequences.

Maximum-likelihood (ML) analyses were performed with the RAxML 7.2.8 program (Stamatakis 2006) under the GTR + Γ model and CAT approximation (25 rate categories per site). The procedure included 100 independent runs of the ML analysis and 1,000 replicates of multiparametric bootstrap. Bayesian inference (BI) analyses were conducted with the MrBayes 3.2.6 program (Ronquist and Huelsenbeck 2003) under GTR + Γ + I model with eight categories of discrete gamma distribution. The program was set to operate under the following parameters: nst = 6, ngammacat = 6, rates = invgamma; the parameters of Metropolis Coupling Marcov Chains Monte Carlo (mcmc): nchains = 4, nruns = 4, temp = 0.2, ngen = 10,000,000, samplefreq = 1,000, burninfrac = 0.5 (the first 50% of the 20,000 sampled trees, i.e., the first 5,000, were discarded in each run). The following averages and standard deviations of split frequencies were obtained: 0.014059 for the SSU rDNA analysis, 0.001084 for the LSU rDNA analysis, and 0.001113 for the ribosomal operon concatenated analysis. The calculations of bootstrap support for the resulting Bayesian trees were performed with the use of the RAxML 7.2.8 program under the same parameters as for the ML analyses (see above).

Alternative tree topologies were manually created and edited with the use the TreeView 1.6.6 program (Page 1996). The reference trees topologies of SSU rDNA (128-taxon dataset), LSU rDNA, and ribosomal operons (53-taxon datasets each) were copied from the trees showed in Figures 7 and 8. Alternative topologies of SSU rDNA phylogenies were constructed by combining all *Selenidium*-like archigregarines in a single clade (see Fig. 9A) followed by positioning this clade within the sporozoans clade successively as a sister group to the cryptosporidians and eugregarine clades Eg1 and Eg2 under assumptions of either their monophyly or polyphyly, or as a sister group to the combined clade cryptosporidians + eugregarines (monophyletic or polyphyletic variants). The eugregarine clades Eg1 and Eg2 were picked out as repeatedly recovered in the reference trees and published phylogenies. Alternative topologies of LSU rDNA and ribosomal operon phylogenies were constructed in the same way, but with the use of the only archigregarine sequence (*S. pygospionis* from *P. elegans*) available to date. Topology tests were performed in Moscow State University with TREE-PUZZLE 5.3.rc16 and CONSEL 0.1j programs (Schmidt et al. 2002; Shimodaira and Hasegawa 2001). The following tests were used: bootstrap probability (Felsenstein 1985); expected-likelihood weights (Strimmer and Rambaut 2002); Kishino–Hasegawa test (Kishino and Hasegawa 1989); Shimodaira–Hasegawa test (Shimodaira and Hasegawa 1999); weighted Shimodaira–Hasegawa Test (Shimodaira and Hasegawa 1999); approximately unbiased test (Shimodaira 2002).

Acknowledgements

This work was supported by St Petersburg State University [grant numbers 1.42.723.2017, 1.42.739.2017]; the Russian Foundation for Basic Research [grant numbers 15-29-02601, 15-04-08870, 15-34-51175, 16-34-50265, 18-04-00324, 18-04-01359]; the Czech Science Foundation [project number GBP505/12/G112 (ECIP – Centre of excellence)]. Ultrastructural and molecular studies of *S. pherusae* were supported by the Russian Science Foundation [project number 18-04-00123]; the molecular study of *S. pygospionis* – by the Russian Science Foundation [project number 14-50-00029]. To make phylogenetic computations, the CIPRES Science Gateway (Miller et al. 2010) and the Supercomputer Center of Lomonosov Moscow State University (http://parallel.ru/cluster) were used in this study. The authors would like to thank the staff of the Marine Biological Station of St Petersburg State University, the White Sea Biological Station of Moscow State University, and Vostok biological station of the National Scientific Center of Marine Biology, Russian Academy of Sciences, for providing facilities for field sampling and material processing, as well as for their kind and friendly

approach. TGS is deeply grateful to Dr. Vasily I. Radashevsky (National Scientific Center of Marine Biology, Russian Academy of Sciences), who first detected the parasites of *Polydora glycymerica* and helped with the sampling of the hosts, and to Profs. Andrey V. Adrianov and Vladimir. V. Yushin from the same institute for their help in organizing the trip to Vostok biological station. GGP and TSM utilized equipment of the core facility centers of St Petersburg State University: "Molecular and Cell Technologies" for electron microscopy and "Observatory of Environmental Safety" for culturing of the marine invertebrates. AD, MK and AV are grateful to the Laboratory of Electron Microscopy, Biology Centre CAS, an institution supported by the Czech-BioImaging large RI project (LM2015062 funded by MEYS CR), for their help with obtaining some EM data. TGS utilized equipment of the Electron microscopy laboratory of the Faculty of Biology and the Center of microscopy of the White Sea Biological station, Lomonosov Moscow State University.

Appendix A. Supplementary Data

Supplementary data associated with this article can be found, in the online version, at https://doi.org/10.1016/j.protis.2018.06.004.

References

Adl SM, Simpson AG, Lane CE, Lukeš J, Bass D, Bowser SS, Brown M, Burki F, Dunthorn M, Hampl V, Heiss A, Hoppenrath M, Lara E, Gall LL, Lynn DH, McManus H, Mitchell EAD, Mozley-Stanridge SE, Parfrey LW, Pawlowski J, Rueckert S, Shadwick L, Schoch C, Smirnov A, Spiegel FW (2012) The revised classification of eukaryotes. J Eukaryot Microbiol **59**:429–514

Bogolepova II (1953) Gregarines of Peter the Great Bay. Trav Inst Zool Acad Sci URSS **13**:38–56 (in Russian)

Butaeva F, Paskerova G, Entzeroth R (2006) *Ditrypanocystis sp*. (Apicomplexa, Gregarinia, Selenidiidae): the mode of survival in the gut of *Enchytraeus albidus* (Annelida, Oligochaeta, Enchytraeidae) is close to that of the coccidian genus C*ryptosporidium*. Tsytologiya **48**:695–704

Castellon C, Gracia MP (1988) *Lecudina capensis* sp. n. parasitic gregarine of *Pherusa laevis* (Stimpson, 1856) (polychaete annelid). Acta Protozool **27**:291–296

Caullery M, Mesnil F (1899) Sur quelques parasites internes des Annélides. Trav Sta Zool Wimereux **7**:80–99

Caullery M, Mesnil F (1901) Le parasitisme intracellulaire et la multiplication asexuée des grégarines. C R Hebd Séanc Mém Soc Biol Paris **53**:84–87

Cavalier-Smith T (2014) Gregarine site-heterogeneous 18S rDNA trees, revision of gregarine higher classification, and the evolutionary diversification of Sporozoa. Europ J Protistol **50**:472–495

Cavalier-Smith T, Chao EE (2004) Protalveolate phylogeny and systematics and the origins of Sporozoa and dinoflagellates (phylum Myzozoa nom. nov.). Europ J Protistol **40**:185–212

Cox FEG (1994) The evolutionary expansion of the Sporozoa. Int J Parasitol **24**:1301–1316

de Faria G, da Cunha AB, da Fonseca OR (1917) Sobre es protozoarios parasitos da *Polydora socialis*. Brazil Med **31**:243

Desportes I, Schrével J (eds) Treatise on Zoology—Anatomy, Taxonomy, Biology. The Gregarines (2 vols). The early branching Apicomplexa. Brill Leiden, Boston, 781 p

Dibb MJ (1938) *Selenocystis foliata* (Ray) from *Scolelepis fuliginosa* Clpde. and its identity with *Haplozoon* sp. Parasitology **30**:296–308

Douglass TG, Jones I (1991) Parasites of California spionid polychaetes. Bull Mar Sci **48**:308–317

Edgar RC (2004) MUSCLE: multiple sequence alignment with high accuracy and high throughput. Nucleic Acids Res **35**:1792–1797

Felsenstein J (1985) Confidence limits on phylogenies: an approach using the bootstrap. Evolution **39**:783–791

Floyd RM, Abebe E, Papert A, Blaxter ML (2002) Molecular barcodes for soil nematode identification. Mol Ecol **11**:839–850

Fowell (1936a) Observations on the Sporozoa inhabiting the gut of the polychaete worm *Polydora flava* Claparède. J Parasitol **28**:414–430

Fowell (1936b) The fibrillar structures of protozoa, with special reference to schizogregarines of the genus *Selenidium*. J Roy Microsc Soc **56**:12–28

Ganapati PN (1946) Notes on some gregarines from polychaetes of the Madras coast. Proc Ind Acad Sci Sect B **23**:228–248

Giard A (1884) Note sur un nouveau groupe de protozaires parasites des annélides, et sur quelques points de l'histoire des grégarines (*Selenidium pendula*). Association française pour l'avancement des sciences. Congres de Blois, 1884. Première partie. Documents officiels, procès-verbaux **1**:192

Grassé PP (1953) Classe des Grégarinomorphes. In Grassé PP (ed) Traité de Zoologie. Masson, Paris, pp 550–690

Gunderson J, Small EB (1986) *Selenidium vivax* n. sp. (Protozoa, Apicomplexa) from the sipunculid *Phascolosoma agassizii* Keferstein, 1867. J Parasitol **72**:107–110

Hall TA (1999) BioEdit: a user-friendly biological sequence alignment editor and analysis program for Windows 95/98/NT. Nucleic Acids Symp Ser **41**:95–98

Janouškovec J, Tikhonenkov DV, Burki F, Howe AT, Kolísko M, Mylnikov AP, Keeling PJ (2015) Factors mediating plastid dependency and the origins of parasitism in apicomplexans and their close relatives. Proc Natl Acad Sci USA **112**:10200–10207

Kishino H, Hasegawa M (1989) Evaluation of the maximum likelihood estimate of the evolutionary tree topologies from DNA sequence data, and the branching order in hominoidea. J Mol Evol **29**:170–179

Kuvardina ON, Simdyanov TG (2002) Fine structure of syzygy in *Selenidium pennatum* (Sporozoa, Archigregarinida). Protistology **2**:169–177

Leander BS (2006) Ultrastructure of the archigregarine *Selenidium vivax* (Apicomplexa)—A dynamic parasite of sipunculid worms (host: *Phascolosoma agassizii*). Mar Biol Res **2**:178–190

Leander BS (2007) Molecular phylogeny and ultrastructure of *Selenidium serpulae* (Apicomplexa, Archigregarinia) from the calcareous tubeworm *Serpula vermicularis* (Annelida, Polychaeta, Sabellida). Zool Scr **36**:213–227

Leander BS (2008a) Marine gregarines: evolutionary prelude to the apicomplexan radiation? Trends Parasitol **24**:60–67

Leander BS (2008b) A hierarchical view of convergent evolution in microbial eukaryotes. J Eukaryot Microbiol **55**:59–68

Leander BS, Keeling PJ (2003) Morphostasis in alveolate evolution. Trends Ecol Evol **18**:395–402

Lepelletier F, Karpov SA, Le Panse S, Bigeard E, Skovgaard A, Jeanthon C, Guillou L (2014) *Parvilucifera rostrata* sp. nov. (Perkinsozoa), a novel parasitoid that infects planktonic dinoflagellates. Protist **165**:31–49

Levine ND (1971) Taxonomy of the Archigregarinorida and Selenidiidae (Protozoa, Apicomplexa). J Protozool **18**:704–717

Levine ND (1985) Phylum 2. Apicomplexa Levine, 1970. In Lee JJ, Hutner SH, Bovee EC (eds) An Illustrated Guide to the Protozoa. Society of Protozoologists, Kansas, pp 322–374

MacGregor HC, Thomasson PA (1965) The fine structure of two archigregarines, *Selenidium fallax* and *Ditrypanocystis cirratuli*. J Protozool **12**:438–443

Mellor JS, Stebbings H (1980) Microtubules and the propagation of bending waves by the archigregarine, *Selenidium fallax*. J Exp Biol **87**:149–161

Mikhailov KV, Simdyanov TG, Aleoshin VV (2017) Genomic survey of a hyperparasitic microsporidian *Amphiamblys* sp. (Metchnikovellidae). Genome Biol Evol **9**:454–467

Miller MA, Pfeiffer W, Schwartz T (2010) In Creating the CIPRES Science Gateway for inference of large phylogenetic trees. Gateway Computing Environments Workshop (GCE) : pp 1–8

Page RDM (1996) TREEVIEW: An application to display phylogenetic trees on personal computers. Comp Appl Biosci **12**:357–358

Paskerova GG, Frolova EV, Kováčiková M, Panfilkina TS, Mesentsev ES, Smirnov AV, Nassonova ES (2016) *Metchnikovella dogieli* sp. n (Microsporidia: Metchnikovellida), a parasite of archigregarines *Selenidium* sp. from polychaetes *Pygospio elegans*. Protistology **10**:148–157

Perkins FO, Barta JR, Clopton RE, Peirce MA, Upton SJ (2000) Phylum Apicomplexa Levine, 1070. In Lee JJ, Leedale GF, Bradbury P (eds) An Illustrated Guide to the Protozoa **Vol 1**, 2nd edn Society of Protozoologists, Lawrence, Kansas, USA, pp 190–370

Ray HN (1930) Studies on some Sporozoa in polychaete worms. I. Gregarines of the genus *Selenidium*. J Parasitol **22**:370–398

Reichenow E (1932) Sporozoa. In Grimpe G, Wagler E (eds) Die Tierwelt der Nord und Ostsee. Leipzig, Lief 21 (Teil II), pp 1–88

Ronquist F, Huelsenbeck JP (2003) MrBayes 3: Bayesian phylogenetic inference under mixed models. Bioinformatics **19**:1572–1574

Rotari YM, Paskerova GG, Sokolova YY (2015) Diversity of metchnikovellids (Metchnikovellidae, Rudimicrosporea), hyperparasites of bristle worms (Annelida, Polychaeta) from the White Sea. Protistology **9**:50–59

Rueckert S, Horák A (2017) Archigregarines of the English Channel revisited: New molecular data on *Selenidium* species including early described and new species and the uncertainties of phylogenetic relationships. PLoS ONE **12**:e0187430

Rueckert S, Leander BS (2009) Molecular phylogeny and surface morphology of marine archigregarines (Apicomplexa), *Selenidium* spp. , *Filipodium phascolosomae* n. sp. and *Platyproteum* n. g. and comb. from North-Eastern Pacific peanut worms (Sipuncula). J Eukaryot Microbiol **56**:428–439

Rueckert S, Simdyanov TG, Aleoshin VV, Leander BS (2011) Identification of a divergent environmental DNA sequence clade using the phylogeny of gregarine parasites (Apicomplexa) from crustacean hosts. PLoS ONE **6**:e18163

Schmidt HA, Strimmer K, Vingron M, von Haeseler A (2002) TREE-PUZZLE: maximum likelihood phylogenetic analysis using quartets and parallel computing. Bioinformatics **18**:502–504

Schrével J (1966) Cycle de *Selenidium pendula* Giard, 1884, gregarine parasite de *Nerine cirratulus* delle Chiaje (annelide polychete). Protistologica **2**:31–34

Schrével J (1967) Mouvements chez les grégarines. SFRS-CERIMES. www.canal-u.tv/video/cerimes/mouvements_chezle sgregarines.13331

Schrével J (1968) L'ultrastructure de la region aterieure de la Gregarine *Selenidium* et son interet pour l'etude de la nutrition chez les Sporozoaires. J Microsc **7**:391–410

Schrével J (1970) Contribution à l'étude des Selenidiidae parasites d'annélides polychètes. 1.—Cycle biologiques. Protistologica **6**:389–426

Schrével J (1971a) Contribution à l'étude des Selenidiidae parasites d'annélides polychètes. II. Ultrastructure de quelques trophozoites. Protistologica **7**:101–130

Schrével J (1971b) Observations biologiques et ultrastructurales sur les Selenidiidae et leurs conséquences sur la systématique des Grégarinomorphes. J Protozool **18**:448–479

Schrével JS, Buissonnet S, Metais MM (1974) Action de l'uree sur la motilite et les microtubules sous-pelliculaires de Protozoaire *Selenidium hollandei*. C R Acad Sc Paris **278**:2201–2204

Schrével J, Valigurová A, Prensier G, Chambouvet A, Florent I, Guillou L (2016) Ultrastructure of *Selenidium pendula*, the type species of archigregarines, and phylogenetic relations to other marine Apicomplexa. Protist **167**:339–368

Shimodaira H (2002) An approximately unbiased test of phylogenetic tree selection. Syst Biol **51**:492–508

Shimodaira H, Hasegawa M (1999) Multiple comparisons of log-likelihoods with applications to phylogenetic inference. Mol Biol Evol **16**:1114–1116

Shimodaira H, Hasegawa M (2001) CONSEL: for assessing the confidence of phylogenetic tree selection. Bioinformatics **17**:1246–1247

Simdyanov TG (1992) *Selenidium pennatum* sp. n., a new species of archigregarines from *Flabelligera affinis* (Polychaete: Flbelligeridae). Parazitologiya **4**:344–347 (in Russian with English summary)

Simdyanov TG, Kuvardina ON (2007) Fine structure and putative feeding mechanism of the archigregarine *Selenidium orientale* (Apicomplexa: Gregarinomorpha). Europ J Protistol **43**:17–25

Simdyanov TG, Diakin AY, Aleoshin VV (2015) Ultrastructure and 28S rDNA phylogeny of two gregarines: *Cephaloidophora cf. communis* and *Heliospora cf. longissima* with remarks on gregarine morphology and phylogenetic analysis. Acta Protozool **54**:241–262

Simdyanov TG, Guillou L, Diakin AY, Mikhailov KV, Schrével J, Aleoshin VV (2017) A new view on the morphology and phylogeny of eugregarines suggested by the evidence from the gregarine *Ancora sagittata* (Leuckart, 1860) Labbé, 1899 (Apicomplexa: Eugregarinida). PeerJ **5**:e3354 https://peerj.com/articles/3354/

Sokolova YY, Paskerova GG, Rotari YM, Nasonova ES, Smirnov AV (2013) Fine structure of *Metchnikovella incurvata* Caullery and Mesnil 1914 (microsporidia), a hyperparasite of gregarines *Polyrhabdina sp.* from the polychaete *Pygospio elegans*. Parasitology **140**:855–867

Sokolova YY, Paskerova GG, Rotari YM, Nassonova ES, Smirnov AV (2014) Description of *Metchnikovella spiralis* sp. n (Microsporidia: Metchnikovellidae), with notes on the ultrastructure of metchnikovellids. Parasitology **141**:1108–1122

Stamatakis A (2006) RAxML-VI-HPC: maximum likelihood-based phylogenetic analyses with thousands of taxa and mixed models. Bioinformatics **22**:2688–2690

Stebbings H, Boe GS, Garlick PR (1974) Microtubules and movement in the archigregarine, *Selenidium fallax*. Cell Tissue Res **148**:331–345

Strimmer K, Rambaut A (2002) Inferring confidence sets of possibly misspecified gene trees. Proc R Soc Lond B **269**:137–142

Tuzet O, Ormières R (1958) *Selenidium flabelligerae* n. sp. parasite de *Flabelligera diplochaitos* Otto (Annélide sédentaire). Ann Sci Nat Zool Ser **11(20)**:71–76

Tuzet O, Ormières R (1965) *Selenidium productum* nom. nov. pour *Selenidium flabelligerae* Tuz. et Orm., 1958, preémployé. Vie et Milieu **15**:801–802

Valigurová A, Vaškovicová N, Diakin A, Paskerova GG, Simdyanov TG, Kováčiková M (2017) Motility in blastogregarines (Apicomplexa): native and drug-induced organisation of *Siedleckia nematoides* cytoskeletal elements. PLoS ONE **12(6)**:e0179709

Vávra J (1969) *Lankesteria barretti* n. sp. (Eugregarinida, Diplocystidae), a parasite of the mosquito *Aedes triseriatus* (Say) and a review of the genus *Lankesteria* Mingazzini. J Protozool **16**:546–570

Vivier E, Schrével J (1964) Etude au microscope electronique de une gregarine du genre *Selenidium*, parasite de *Sabellaria alveolata* L. J Microscopie Paris **3**:651–670

Vivier E, Schrével J (1966) Les ultrastructures cytoplasmiques de *Selenidium hollandei*, n. sp., Grégarine parasite de *Sabellaria alveolata* L. J Microscopie Paris **5**:213–228

Vivier E, Devauchelle G, Petitprez A, Porchet-Henneré E, Prensier G, Schrével J, Vinckier D (1970) Observations de cytologie comparée chez les sporozoaires. I.—Les structures superficielles chez les formes végétatives. Protistologica **6**:127–150

Wakeman KC, Horiguchi T (2018) Morphology and molecular phylogeny of the marine gregarine parasite *Selenidium oshoroense* n. sp. (Gregarina, Apicomplexa) isolated from a Northwest Pacific *Hydroides ezoensis* Okuda 1934 (Serpulidae, Polychaeta). Mar Biodiv **48**:1489–1498 https://doi.org/10.1007/s12526-017-0643-1

Wakeman KC, Leander BS (2012) Molecular phylogeny of pacific archigregarines (Apicomplexa), including descriptions of *Veloxidium leptosynaptae* n. gen., n. sp., from the sea cucumber *Leptosynapta clarki* (Echinodermata), and two new species of *Selenidium*. J Eukaryot Microbiol **59**:232–245

Wakeman KC, Leander BS (2013) Molecular phylogeny of marine gregarine parasites (Apicomplexa) from tube-forming polychaetes (Sabellariidae, Cirratulidae, and Serpulidae), including descriptions of two new species of *Selenidium*. J Eukaryot Microbiol **60**:514–525

Wakeman KC, Heintzelman MB, Leander BS (2014) Comparative ultrastructure and molecular phylogeny of *Selenidium melongena* n. sp. and *S. terebellae* Ray 1930 demonstrate niche partitioning in marine gregarine parasites (Apicomplexa). Protist **165**:493–511

WoRMS (2018) *Selenidium* Giard, 1884. Accessed through: World Register of Marine Species at http://www.marinespecies.org/aphia.php?p=taxdetails&id=562744 on 2018-03-03